Available online at www.sciencedirect.com
ScienceDirect
ELSEVIER
Coordination Chemistry Reviews 250 (2006) 2176–2193
COORDINATION CHEMISTRY REVIEWS
www.elsevier.com/locate/ccr

Review

Trans-dicyanobis(acetylacetonato)ruthenate(III) as a precursor to build novel cyanide-bridged Ru^{III}–M^{II} bimetallic compounds [M = Co and Ni]

Luminita Marilena Toma [a], Liviu Dan Toma [a], Fernando S. Delgado [b], Catalina Ruiz-Pérez [b], Jorunn Sletten [c], Joan Cano [d], Juan Modesto Clemente-Juan [a], Francesc Lloret [a], Miguel Julve [a,*]

[a] *Departament de Química Inorgànica/Instituto de Ciencia Molecular, Facultat de Química de la Universitat de València, Dr. Moliner 50, 46100 Burjassot (València), Spain*
[b] *Laboratorio de Rayos X y Materiales Moleculares, Departamento de Física Fundamental II, Facultad de Física de la Universidad de La Laguna, Avda. Astrofísico Francisco Sánchez, s/n, 38204 La Laguna (Tenerife), Spain*
[c] *Department of Chemistry, University of Bergen, Allégaten 41, N-5007 Bergen, Norway*
[d] *Institució Catalana de Recerca i Estudis Avançats (ICREA)/Departanment de Química Inorgànica i Centre de Recerca en Química Teòrica, Universitat de Barcelona, Diagonal 647, 08028 Barcelona, Spain*

Received 28 July 2005; accepted 25 November 2005
Available online 7 February 2006

Contents

Abstract

The use of the mononuclear complex *trans*-[Ru(acac)$_2$(CN)$_2$]$^-$ as a ligand towards the preformed species [Ni$_2$L(H$_2$O)$_2$Cl$_2$], [Co(dmphen)](NO$_3$)$_2$, [Ni(dmphen)](NO$_3$)$_2$ and [Co(H$_2$O)$_6$](NO$_3$)$_2$ afforded the novel cyanide-bridged bimetallic compounds of formula [{Ru(acac)$_2$(CN)$_2$}{Ni$_2$(L)(H$_2$O)$_2$}]{Ru(acac)$_2$(CN)$_2$}·2H$_2$O (**1**), [{Ru(acac)$_2$(CN)$_2$}{Co(dmphen)(NO$_3$)}]·H$_2$O (**2**) and [{Ru(acac)$_2$(CN)$_2$}{Ni(dmphen)(NO$_3$)}]·H$_2$O (**3**) and [{Ru(acac)$_2$(CN)$_2$}$_2$Co] (**4**) [Hacac = acetylacetone, dmphen = 2,9-dimethylphenanthroline and H$_2$L = 11,23-dimethyl-3,7,15,19-tetrazatricyclo[19.3.1.1^{9,13}]hexacosa-2,7,9,11,13(26),14,19,21(25),22,24-decaene-25,26-diol]. Their syntheses, X-ray crystal structures and

* Corresponding author. Tel.: +34 96 354 4440; fax: +34 96 354 4322.
E-mail address: miguel.julve@uv.es (M. Julve).

doi:10.1016/j.ccr.2005.11.018

magnetic properties are reported here. The structure of **1** consists of cationic cyanide-bridged chains of formula $[\{Ru(acac)_2(CN)_2\}\{Ni_2(L)(H_2O)_2\}]^+$ and mononuclear anions $[Ru(acac)_2(CN)_2]^-$. Compounds **2** and **3**, which are isostructural, are made up of cyanide-bridged neutral chains $[\{Ru(acac)_2(CN)_2\}\{M(dmphen)(NO_3)\}]$ with regular alternating ruthenium(III) and cobalt(II) (**2**)/nickel(II) (**3**) ions. Each cobalt atom in **4** is tetrahedrally coordinated by four $[Ru^{III}(acac)_2(CN)_2]^-$ ions through the cyano nitrogen atoms to afford a two-fold interpenetrated (6,4) three-dimensional network which is formed by 12 gon cycles having six ruthenium and six cobalt atoms. The metal–metal separations through the cyanide bridge are 5.2491(1) Å for **1**, 5.2038(12) and 5.2426(12) Å for **2**, 5.2130(12) and 5.2253(12) Å for **3** and 5.1155(15) and 5.1100(15) Å for **4**. The magnetic properties of **1**–**4** together with those of the mononuclear precursor *trans*-$PPh_4[Ru(acac)_2(CN)_2]$ (PPh_4^+ = tetraphenylphosphonium cation and Hacac = acetylacetone) were investigated in the temperature range 1.9–295 K. The cyano-bearing ruthenium(III) precursor exhibits the magnetic behavior expected for a low-spin distorted octahedral ruthenium(III) system with spin-orbit coupling of the $^2T_{2g}$ ground term. Compound **1** exhibits an overall antiferromagnetic behavior, the magnetic coupling between the nickel(II) ions through the double phenoxo group and that between adjacent ruthenium(III) and nickel(II) centers through the single cyano bridge being −50.0 and +6.6 cm^{-1}, respectively. Compounds **2** and **3** behave as ferromagnetic chains. The intrachain magnetic coupling in **3** is +3.2 cm^{-1} whereas that in **2** could not be evaluated because of the lack of a suitable model. No magnetic ordering is observed in **2** and **3** down to 1.9 K. Compound **4** shows an overall ferromagnetic behavior and it exhibits ferromagnetic ordering at T_c = 5.4 K. Theoretical calculations based on density functional theory (DFT) have been employed on the *trans*-$[Ru(acac)_2(CN)_2]^-$ mononuclear complex and on dinuclear fragments of the compounds **1**–**3** in order to analyze the efficiency of the exchange pathways through the double phenoxo (**1**) and single cyano bridge (**1**–**3**) and to substantiate the exchange coupling parameters involved.

Keywords: Ruthenium(III) complexes; Nickel(II) complexes; Cobalt(II) complexes; Bimetallic chains; Interpenetrated three-dimensional network; Magnetic properties; Magnetic ordering

1. Introduction

A well known approach to the preparation of molecule-based magnets which can exhibit interesting electrochemical, optical and photophysical properties consists of using the paramagnetic building block $[M(CN)_6]^{(6-m)-}$ (M = di- or trivalent first-row transition metal ion) as a ligand towards fully solvated metal ions [1–23]. The recent achievement of ordering temperatures at/or above room temperature in these cyano-bridged compounds by following rational synthetic strategies has been one of the more important results in molecular magnetism [6,8,10]. The large amount of magneto-structural results obtained by using these hexacyanometallates as precursors contrasts with the paucity of results dealing with the related precursors containing 4d or 5d metal ions. The more diffuse character of the 4d and 5d type orbitals would lead to an enhancement of the magnetic interactions in the corresponding cyanide-bridged compounds. In addition, the synthetic chemist can take advantage of the more substitution-inert character of these heavier precursors.

Looking at the impressive work performed with the robust and readily available low-spin complex $[Fe(CN)_6]^{3-}$ ($S_{Fe} = \frac{1}{2}$) when used as a ligand [2–4,24–41], an appealing candidate could be the related building block $[Ru(CN)_6]^{3-}$ ($S_{Ru} = \frac{1}{2}$). In fact, theoretical calculations on $[Fe(CN)_6]^{3-}$ and $[Ru(CN)_6]^{3-}$ anions reveal significantly higher spin densities on the cyanide ligands in the ruthenium unit [42] and thus, stronger magnetic interactions are expected through the cyanide ligand in the corresponding cyanide-bridged ruthenium-based heterometallic species. In fact, although the $[Ru(CN)_6]^{3-}$ entity has been known for more than 50 years [43], its structure as a tetraphenylarsonium salt was reported only in 2003 [42]. The instability of its solutions in common polar solvents (water and alcohols) is the reason for the poor knowledge of its coordination chemistry [44]. This accounts for the attempts to design alternative stable cyanide-bearing ruthenium(III) complexes such as the *trans*-$Ph_4P[Ru(acac)_2(CN)_2]$ (PPh_4^+ = tetraphenylphosphonium cation and Hacac = acetylacetone) whose use as a ligand towards fully solvated manganese(II) ions afforded the diamond-like cyano-bridged bimetallic compound of formula $\{Mn[Ru(acac)_2(CN)_2]\}_n$ which exhibits ferromagnetic ordering at T_c = 3.6 K [45].

In this study, we show how the use of the *trans*-bis(acetylacetonato)dicyanoruthenate(III) unit as a ligand toward the partially blocked complexes $[Ni_2L(H_2O)_2Cl_2]$, $[Co(dmphen)](NO_3)_2$, $[Ni(dmphen)](NO_3)_2$ and the fully hydrated cobalt(II) salt $[Co(H_2O)_6](NO_3)_2$ produces the novel cyanide-bridged bimetallic compounds of formula $[\{Ru(acac)_2(CN)_2\}\{Ni_2(L)(H_2O)_2\}]\{Ru(acac)_2(CN)_2\}\cdot 2H_2O$ (**1**), $[\{Ru(acac)_2(CN)_2\}\{Co(dmphen)(NO_3)\}]\cdot H_2O$ (**2**) and $[\{Ru(acac)_2(CN)_2\}\{Ni(dmphen)(NO_3)\}]\cdot H_2O$ (**3**) and $[\{Ru(acac)_2(CN)_2\}_2Co]$ (**4**) [dmphen = 2,9-dimethylphenanthroline and H_2L = 11,23-dimethyl-3,7,15,19-tetrazatricyclo[19.3.1.1^{9,13}]hexacosa-2,7,9,11,13(26),14,19,21(25),22,24-decaene-25,26-diol], see Scheme 1. Their preparation, X-ray crystal structures and variable-temperature magnetic properties are the subject of the present report.

2. Experimental

2.1. Materials

Chemicals were purchased from commercial sources as reagents pure for analysis and they were used as received. The complexes *trans*-$PPh_4[Ru(acac)_2(CN)_2]$ and $[Ni_2^{II}L(H_2O)_2Cl_2]$ were prepared by following previously reported procedures [45–47]. $Ni_2L(H_2O)_2(ClO_4)_2$ was prepared by the reaction of aqueous solutions of $[Ni_2(L)(H_2O)_2Cl_2]$ (1 mmol) and silver perchlorate (2 mmol) in the darkness. After stirring for 5 h, the white precipitate of silver chloride was removed by filtration and discarded. The perchlorate salt was

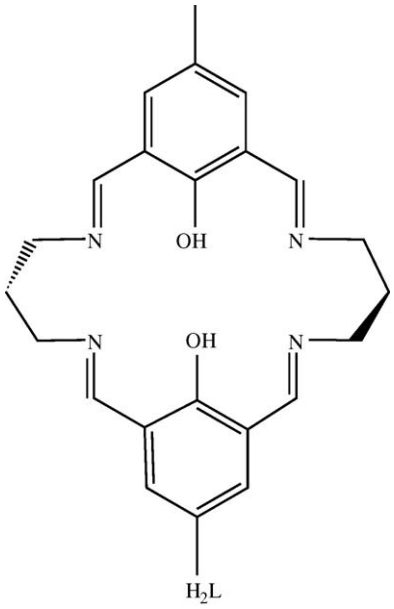

Scheme 1.

obtained as a green polycrystalline powder by slow evaporation of the mother liquor at room temperature. Elemental analysis (C, H, N) was performed by the Microanalytical Service of the Universidad Autónoma de Madrid. Values of 1:1 for the Ru:M [M = Ni (**1** and **3**) and Co (**2**)] and of 2:1 for the Ru:Co (**4**) molar ratios were determined by electron probe X-ray microanalysis at the Servicio Interdepartamental of the University of Valencia.

2.2. Syntheses

2.2.1. $[\{Ru(acac)_2(CN)_2\}\{Ni_2(L)(H_2O)_2\}]\{Ru(acac)_2(CN)_2\}\cdot 2H_2O$ (*1*)

Single crystals of **1** were grown by a slow diffusion method using an H-shaped glass vessel. The starting solutions were methanolic solutions of *trans*-$PPh_4[Ru(acac)_2(CN)_2]$ (0.033 mmol) in one arm and of $Ni_2^{II}L(H_2O)_2(ClO_4)_2$ (0.033 mmol) at the other one. A few weeks later after careful filling of the H-tube with methanol, dark violet prisms of **1** were formed at ambient temperature. The crystals were collected and dried on filter paper. Yield: ca. 40%. Anal. Calc. for $C_{48}H_{62}N_8Ni_2O_{14}Ru_2$ (**1**): C, 44.53; H, 4.83; N, 8.66. Found: C, 47.07; H, 3.98; N, 9.12%. IR stretching cyanide (KBr), cm^{-1}: 2115 m.

2.2.2. $[\{Ru(acac)_2(CN)_2\}\{Co(dmphen)(NO_3)\}]\cdot H_2O$ (*2*) and $[\{Ru(acac)_2(CN)_2\}\{Ni(dmphen)(NO_3)\}]\cdot H_2O$ (*3*)

Single crystals of **2** and **3** were also grown by the procedure used for **1**. In the present case, the starting solutions were a methanolic solution of *trans*-$PPh_4[Ru(acac)_2(CN)_2]$ (0.033 mmol) in one arm (**2** and **3**) and methanol:water 2:1 (v/v) mixture containing $M^{II}(dmphen)(NO_3)_2$ (0.033 mmol) [prepared in situ by stoichiometric reaction between $M(NO_3)_2\cdot 6H_2O$ and dmphen with M = Co (**2**) and Ni (**3**)] in the other one. Methanol was used as the diffusion liquid. Blue (**2**) and violet (**3**) cubes were formed after a few weeks at ambient temperature. The crystals were collected and dried on filter paper. Yield: ca. 45% (**2** and **3**). Anal. Calc. for $C_{26}H_{28}CoN_5O_8Ru$ (**2**): C, 44.71; H, 4.04; N, 10.03. Found: C, 46.67; H, 4.78; N, 9.46%. Anal. Calc. For $C_{26}H_{28}NiN_5O_8Ru$ (**3**): C, 44.73; H, 4.01; N, 10.03. Found: C, 44.49; H, 3.90; N, 9.95%. IR stretching cyanide (KBr), cm^{-1}: 2128 m (**2**) and 2137 m (**3**).

2.2.3. $[\{Ru(acac)_2(CN)_2\}_2Co]$ (*4*)

X-ray quality crystals of **4** were also grown in an H-shaped tube by slow diffusion of methanolic solutions containing *trans*-$PPh_4[Ru(acac)_2(CN)_2]$ (0.033 mmol) in one arm and $Co(NO_3)_2\cdot 6H_2O$ (0.033 mmol) in the other one. Blue prisms of **4** were formed on standing at room temperature after 3 weeks. The yield is about 40%. Anal. Calc. for $C_{24}H_{32}CoN_4O_8Ru_2$ (**2**): C, 37.66; H, 4.21; N, 7.33. Found: C, 38.62; H, 5.02; N, 8.67%. IR stretching cyanide (KBr), cm^{-1}: 2127 m (**4**).

2.3. Physical measurements

The IR spectra (KBr pellets) were performed on a Nicolet Avatar 320 FT-IR spectrophotometer. Magnetic susceptibility measurements on polycrystalline samples of the mononuclear complex *trans*-$PPh_4[Ru(acac)_2(CN)_2]$ and **1**–**4** were carried out with a Quantum Design SQUID magnetometer in the temperature range 1.9–300 K and under applied magnetic fields ranging from 50 G to 1 T. Magnetization versus magnetic field measurements of **1**–**4** were carried out at 2.0 K in the field range 0–5 T. Diamagnetic corrections of the constituent atoms were estimated from Pascal constants [48] as -414×10^{-6} (mononuclear precursor), -623×10^{-6} (**1**), -348×10^{-6} (**2** and **3**) and -318×10^{-6} (**4**) [per one (the mononuclear precursor, **2** and **3**) and two (**1** and **4**) mol of Ru(III)].

2.4. Computational details

The theoretical calculations were carried out with the hybrid B3LYP method [49–51], implemented in the Gaussian 03 program [52]. In order to choose the appropriate basis sets for the ruthenium atom, several calculations were carried out on the mononuclear *trans*-$[Ru^{III}(acac)_2(CN)_2]^-$ complex (see **I** in Fig. 19). We have used Los Alamos (LanL2DZ) and Stuttgart/Dresden (SDD) electron core potentials (ECP) basis sets [53,54] for the ruthenium atom. The valence electrons in these basis sets are described by a double-ζ functions and the core electrons by potential functions. Also, one all-electron double-ζ (3-21G) basis set proposed by Dobbs and Hehre was used [55]. Several ECP (LanL2DZ, SDD) and all-electron double-ζ (3-21G and SV) and triple-ζ (6-31G and TZV) quality basis sets were used for the remaining atoms [56–61]. Different combinations of basis sets have been used, but only a correct description for the doublet spin state of the complex *trans*-$[Ru^{III}(acac)_2(CN)_2]^-$ (**I** in Fig. 19) was found when the 3-21G basis set was used for the ruthenium atom. So, only this basis set was considered in the calculations to evaluate the exchange-coupling constants. For the last purpose, the broken-symmetry approach has been employed to describe the unrestricted solutions of the antiferromagnetic spin states [62–65]. In order to

analyze the magnetic interactions between the metal ions in **1**–**3**, several dinuclear and trinuclear models (**II**–**V** in Fig. 19) have been built from the experimental crystal structures. In some cases, a quadratic convergence method was used to determine the more stable wave functions in the SCF process [66]. Finally, the atomic spin densities were obtained from Natural Bond Orbital (NBO) analysis [67–69].

2.5. Crystallographic data collection and refinement of the structures

Diffraction data were collected with a Bruker-AXS SMART 2 K CCD (**1** and **2**) and a Bruker-Nonius KappaCCD diffractometer (**3** and **4**) at 293 K. Crystal parameters and refinement results are summarized in Table 1. In the case of compound **4** where the crystals are twinned, partial overlapping of diffraction spots made it impossible to collect data from only one of the twins, even when the sample to CCD detector distance was increased to 110 mm. Instead, the approach selected was to decrease the distance to 35 mm in order to measure the combined overlapping spots. The structures were solved by direct methods and refined by full-matrix least-squares based on F^2, including all reflections. Non-hydrogen atoms were anisotropically refined, except crystallization water oxygen in **1** and all atoms in **4**. In compounds **1** and **2**, hydrogen atoms bound to carbon were included in the models at idealized positions, those of coordinated water in **1** were located in a difference Fourier map, and those of crystal water could not be located in either of the compounds. Refinement of hydrogen atoms was performed according to the riding model. The acac and water hydrogen atoms in **3** were located from difference Fourier maps and refined with isotropic temperature factors. The acac groups in compound **4** were disordered over two sites with 0.64:0.46 occupancies, and in this case hydrogen atoms were not included.

The crystal packing in **1** leaves relatively much open space between cation and anion units. There is some electron density (two peaks above 1.0 e $Å^{-3}$) in the voids, and it is possible that this is due to some additional disordered crystal water, but no model could be reasonably fitted.

Data collection and data reduction were done with the SMART and SAINT programs (**1** and **2**) [70] and COLLECT and EVALCCD (**3** and **4**) [71]. Empirical absorption corrections were carried out using SADABS for all compounds [72]. Calculations for structure solution, and refinement were done by standard procedures using WINGX (**3** and **4**) [73], SHELXS-97, SHELXL/PC, SHELX-97 and *XP* programs [74]. The final geometrical calculations of **3** and **4** were carried out with PARST97 [75] and final graphical manipulations of all compounds with CRYSTALMAKER [76] programs. Selected bond distances and angles are listed in Tables 2–5 for (**1**)–(**4**), respectively. CCCD reference numbers are 279523 (**1**), 279524 (**2**), 279525 (**3**) and 279526 (**4**).

3. Results and discussion

3.1. Crystal structure of *1*

The structure of **1** consists of cationic cyanide-bridged Ru^{III}–Ni^{II} chains of formula [{$Ru(acac)_2(CN)_2$}{$Ni_2(L)$

Table 1
Crystal data and structure refinement for [{$Ru(acac)_2(CN)_2$}{$Ni_2(L)(H_2O)_2$}]{$Ru(acac)_2(CN)_2$}·$2H_2O$ (**1**) [{$Ru(acac)_2(CN)_2$}{$Co(dmphen)(NO_3)$}]·H_2O (**2**) [{$Ru(acac)_2(CN)_2$}{$Ni(dmphen)(NO_3)$}]·H_2O (**3**) and [{$Ru(acac)_2(CN)_2$}$_2$Co] (**4**)

	Compound			
	1	**2**	**3**	**4**
Empirical formula	$C_{48}H_{62}Ni_2N_8O_{14}Ru_2$	$C_{26}H_{28}CoN_5O_8Ru$	$C_{26}H_{28}N_5NiO_8Ru$	$C_{24}H_{32}CoN_4O_8Ru_2$
fw	1294.62	698.53	698.29	765.61
T (K)	293(2)	293(2)	293(2)	293(2)
λ (Å)	0.71073	0.71073	0.71073	0.71073
Space group	*P*-1	*P*-1	*P*-1	*P2nm*
a (Å)	10.9719(10)	10.317(2)	10.318(2)	13.342(3)
b (Å)	11.2023(10)	11.328(3)	11.255(2)	12.199(3)
c (Å)	11.6848(11)	13.649(3)	13.658(29)	9.219(3)
α (°)	87.827(2)	103.477(5)	103.66(2)	90
β (°)	86.995(2)	99.826(5)	100.11(2)	90
γ (°)	75.919(2)	107.327(5)	107.468(1)	90
V ($Å^3$)	1390.6(2)	1430(5)	1417.3(6)	1500.5(7)
Z	1	2	2	2
ρ (Mg m^{-3})	1.546	1.622	1.621	1.695
μ (mm^{-1})	1.267	1.164	1.242	1.589
2θ (°)	4.6–64.0	4.3–50.2	12.8–50.3	2.0–55.0
Reflections collected	12940	8755	12539	9558
Independent reflections	8656 [R(int) = 0.0141]	5053 [R(int) = 0.0406]	4882 [R(int) = 0.0780]	3165 [R(int) = 0.0414]
Refl. with $I > 2\sigma(I)$	7034	3516	2916	2653
Data/restraint/parameters	8656/0/337	5053/0/379	4882/0/377	3165/1/145
R^a [$I > 2\sigma(I)$]	0.0377	0.0636	0.0642	0.0663
$R_w{}^b$ [$I > 2\sigma(I)$]	0.1135	0.1544	0.1424	0.1426

[a] $R = \Sigma||F_o| - |F_c||/\Sigma|F_o|$.

[b] $R_w = [\Sigma w(F_o^2 - F_c^2)^2/\Sigma w(F_o^2)^2]^{1/2}$.

Table 2
Selected bond lengths (Å) and angles (°)[a] for **1**

Nickel coordination sphere			
Ni(1)–N(1)	2.006(2)	Ni(1)–O(1)	2.0318(16)
Ni(1)–N(2a)	2.026(2)	Ni(1)–N(3)	2.096(2)
Ni(1)–O(1a)	2.091(17)	Ni(1)–O(2)	2.1909(19)
N(1)–Ni(1)–N(2a)	98.53(9)	O(1a)–Ni(1)–N(3)	90.87(8)
N(1)–Ni(1)–O(1a)	169.29(8)	O(1)–Ni(1)–N(3)	93.42(8)
N(2a)–Ni(1)–O(1a)	91.44(8)	N(1)–Ni(1)–O(2)	88.56(9)
N(1)–Ni(1)–O(1)	90.63(8)	N(2a)–Ni(1)–O(2)	87.99(8)
N(2a)–Ni(1)–O(1)	169.17(8)	O(1a)–Ni(1)–O(2)	87.90(7)
O(1a)–Ni(1)–O(1)	79.07(7)	O(1)–Ni(1)–O(2)	86.48(7)
N(1)–Ni(1)–N(3)	92.67(9)	N(3)–Ni(1)–O(2)	178.77(9)
N(2a)–Ni(1)–N(3)	91.91(9)		
Ruthenium coordination sphere			
Ru(1)–O(4)	2.000(2)	Ru(2)–O(6)	2.0061(19)
Ru(1)–O(3)	2.007(2)	Ru(2)–O(5)	2.007(2)
Ru(1)–C(18)	2.066(3)	Ru(2)–C(24)	2.066(3)
O(4b)–Ru(1)–O(4)	180.00(15)	O(6c)–Ru(2)–O(6)	180.000(1)
O(4)–Ru(1)–O(3)	90.24(13)	O(6)–Ru(2)–O(5c)	89.45(9)
O(4)–Ru(1)–O(3b)	89.76(13)	O(6)–Ru(2)–O(5)	90.55(9)
O(3)–Ru(1)–O(3b)	180.00(19)	O(5c)–Ru(2)–O(5)	180.000(1)
O(4)–Ru(1)–C(18b)	88.25(10)	O(6)–Ru(2)–C(24)	89.62(10)
O(3)–Ru(1)–C(18b)	87.43(10)	O(5)–Ru(2)–C(24)	87.37(11)
O(4)–Ru(1)–C(18)	91.75(10)	O(6)–Ru(2)–C(24c)	90.38(10)
O(3)–Ru(1)–C(18)	92.57(10)	O(5)–Ru(2)–C(24c)	96.63(11)
C(18c)–Ru(1)–C(18)	180.00(15)	C(24)–Ru(2)–C(24c)	180.000(1)
Cyano ligands			
N(3)–C(18)	1.146(3)	N(4)–C(24)	1.142(4)
C(18)–N(3)–Ni(1)	166.4(3)	N(4)–C(24)–Ru(2)	178.0(3)
N(3)–C(18)–Ru(1)	174.3(2)		
Acac ligands			
O(3)–C(14)	1.303(5)	O(5)–C(20)	1.266(4)
O(4)–C(16)	1.263(5)	O(6)–C(22)	1.278(4)
C(13)–C(14)	1.505(7)	C(19)–C(20)	1.512(5)
C(14)–C(15)	1.394(8)	C(20)–C(21)	1.391(5)
C(15)–C(16)	1.338(8)	C(21)–C(22)	1.378(5)
C(16)–C(17)	1.493(7)	C(22)–C(23)	1.506(5)
C(14)–O(3)–Ru(1)	121.7(3)	O(4)–C(16)–C(17)	115.4(6)
C(16)–O(4)–Ru(1)	124.0(3)	C(15)–C(16)–C(17)	119.1(5)
C(20)–O(5)–Ru(2)	123.5(2)	O(5)–C(20)–C(21)	125.0(3)
C(22)–O(6)–Ru(2)	123.0(2)	O(5)–C(20)–C(19)	114.9(3)
O(3)–C(14)–C(15)	124.3(4)	C(21)–C(20)–C(19)	120.0(3)
O(3)–C(14)–C(13)	112.3(6)	C(22)–C(21)–C(20)	126.5(3)
C(15)–C(14)–C(13)	123.3(5)	O(6)–C(22)–C(21)	125.6(3)
C(16)–C(15)–C(14)	127.3(4)	O(6)–C(22)–C(23)	113.4(3)
O(4)–C(16)–C(15)	125.4(4)	C(21)–C(22)–C(23)	121.0(3)
L ligand			
O(1)–C(3)	1.305(3)	C(4)–C(11)	1.407(4)
N(1)–C(1)	1.278(3)	C(4)–C(5)	1.450(4)
N(1)–C(8a)	1.470(4)	C(6)–C(7)	1.510(5)
N(2)–C(5)	1.282(3)	C(7)–C(8)	1.499(5)
N(2)–C(86)	1.483(3)	C(8)–N(1a)	1.470(4)
C(1)–C(2)	1.455(4)	C(9)–C(10)	1.378(4)
C(2)–C(9)	1.406(3)	C(10)–C(11)	1.381(4)
C(2)–C(3)	1.416(3)	C(10)–C(12)	1.517(4)
C(3)–C(4)	1.424(3)		
C(3)–O(1)–N(1a)	129.39(15)	N(1)–C(1)–C(2)	127.9(2)
C(3)–O(1)–Ni(1)	128.63(15)	C(9)–C(2)–C(3)	120.4(2)
Ni(1a)–O(1)–Ni(1)	100.93(7)	C(9)–C(2)–C(1)	114.8(2)
C(1)–N(1)–C(8a)	115.6(2)	C(3)–C(2)–C(81)	124.7(2)
C(1)–N(1)–Ni(1)	124.66(18)	O(1)–C(3)–C(2)	121.9(2)
C(8a)–N(1)–Ni(1)	119.71(19)	O(1)–C(3)–C(4)	121.3(2)
C(5)–N(2)–C(6)	115.0(2)	C(2)–C(3)–C(4)	116.9(2)
C(5)–N(2)–Ni(1a)	123.24(18)	C(11)–C(4)–C(3)	119.9(2)
C(6)–N(2)–Ni(1a)	121.60(18)	C(11)–C(4)–C(5)	114.7(2)
C(3)–C(4)–C(5)	125.4(2)	C(10)–C(9)–C(2)	122.8(3)
N(2)–C(5)–C(4)	128.9(2)	C(9)–C(10)–C(11)	116.9(2)
N(2)–C(6)–C(7)	113.3(2)	C(9)–C(10)–C(12)	121.8(3)
C(8)–C(7)–C(6)	115.7(3)	C(11)–C(10)–C(12)	121.3(3)
N(1a)–C(8)–C(7)	112.8(3)	C(10)–C(11)–C(4)	123.0(3)

D	H	A	D···A (Å)	H···A (Å)	D–H···A (°)
Hydrogen bonds[b]					
O(2)	H(01)	N(3a)	3.096(3)	2.25	162
O(2)	H(02)	N(4d)	2.811(3)	2.03	169
O(7)		O(2)	2.923(9)		
O(7)		O(3e)	3.110(9)		

[a] Estimated standard deviations in the last significant digits are given in parentheses. Symmetry transformations: (a) $-x, 1-y, -z$; (b) $-x, -y, -z$; (c) $1-x, 1-y, 1-z$; (d) $x, y, z-1$; (e) $x, 1+y, z$.
[b] A = acceptor, D = donor.

Table 3
Selected bond lengths (Å) and angles (°)[a] for **2**

Cobalt coordination sphere			
Co(1)–N(1)	2.050(6)	Co(1)–N(2)	2.136(6)
Co(1)–N(4)	2.057(5)	Co(1)–O(4)	2.202(6)
Co(1)–N(3)	2.100(5)	Co(1)–O(3)	2.219(6)
N(1)–Co(1)–N(4)	173.9(2)	N(3)–Co(1)–O(4)	109.7(2)
N(1)–Co(1)–N(3)	92.8(2)	N(2)–Co(1)–O(4)	169.7(2)
N(4)–Co(1)–N(3)	91.4(2)	N(1)–Co(1)–O(3)	90.9(2)
N(1)–Co(1)–N(2)	94.3(2)	N(4)–Co(1)–N(3)	84.1(2)
N(4)–Co(1)–N(2)	90.8(2)	N(3)–Co(1)–O(3)	168.2(2)
N(3)–Co(1)–N(2)	78.6(2)	N(2)–Co(1)–O(3)	112.2(3)
N(1)–Co(1)–O(4)	91.3(2)	O(4)–Co(1)–O(3)	59.0(2)
N(4)–Co(1)–O(4)	83.0(2)		
Ruthenium coordination sphere			
Ru(1)–O(2)	2.003(4)	Ru(2)–O(7)	2.005(5)
Ru(1)–O(1)	2.004(5)	Ru(2)–O(6)	2.013(5)
Ru(1)–C(6)	2.071(6)	Ru(2)–C(21)	2.072(8)
O(2)–Ru(1)–O(2a)	180.00(1)	O(7b)–Ru(2)–O(7)	180.0(3)
O(2)–Ru(1)–O(1)	89.9(2)	O(7)–Ru(2)–O(6b)	89.8(2)
O(2a)–Ru(1)–O(1)	90.1(2)	O(7)–Ru(2)–O(6)	90.2(2)
O(1)–Ru(1)–O(1a)	180.0(3)	O(6b)–Ru(2)–O(6)	180.000(2)
O(2)–Ru(1)–C(6)	89.4(2)	O(7)–Ru(2)–C(21b)	86.4(2)
O(2b)–Ru(1)–C(6)	90.6(2)	O(6)–Ru(2)–C(21b)	85.4(2)
O(1)–Ru(1)–C(6)	92.9(2)	O(7)–Ru(2)–C(21)	93.6(2)
O(1)–Ru(1)–C(6a)	87.1(2)	O(6)–Ru(2)–C(21)	94.6(2)
C(6)–Ru(1)–C(6a)	180.0(3)	C(21b)–Ru(2)–C(21)	180.0(3)
Cyano groups			
N(1)–C(6)	1.128(8)	N(4)–C(21)	1.132(9)
C(6)–N(1)–Co(1)	170.2(6)	C(21)–N(4)–Co(1)	176.9(7)
N(1)–C(6)–Ru(1)	172.4(6)	N(4)–C(21)–Ru(2)	172.4(7)
Acac ligands			
O(1)–C(2)	1.279(9)	O(6)–C(23)	1.262(9)
O(2)–C(4)	1.262(9)	O(7)–C(25)	1.266(9)
C(1)–C(2)	1.502(11)	C(22)–C(23)	1.504(11)
C(2)–C(3)	1.382(11)	C(23)–C(24)	1.396(11)
C(3)–C(4)	1.394(11)	C(24)–C(25)	1.390(11)
C(4)–C(5)	1.485(10)	C(25)–C(26)	1.507(12)
C(2)–O(1)–Ru(1)	120.9(5)	C(23)–O(6)–Ru(2)	123.2(5)
C(4)–O(2)–Ru(1)	124.1(5)	C(25)–O(7)–Ru(2)	122.1(5)
O(1)–C(2)–C(3)	125.2(7)	O(6)–C(23)–C(24)	124.9(7)
O(1)–C(2)–C(1)	114.0(8)	O(6)–C(23)–C(19)	114.9(3)
C(3)–C(2)–C(1)	120.8(8)	C(24)–C(23)–C(22)	120.8(8)

Table 3 (*Continued*)

C(2)–C(3)–C(4)	126.1(8)	C(25)–C(24)–C(23)	125.6(8)
O(2)–C(4)–C(3)	123.8(7)	O(7)–C(25)–C(24)	126.1(8)
O(2)–C(4)–C(5)	115.9(7)	O(7)–C(25)–C(26)	113.5(8)
C(3)–C(4)–C(5)	120.3(8)	C(24)–C(25)–C(26)	120.3(8)
Nitrato ligand			
O(3)–N(5)	1.290(11)	O(5)–N(5)	1.234(11)
O(4)–N(5)	1.262(10)		
N(5)–O(3)–Co(1)	90.6(5)	O(5)–N(5)–O(3)	122.5(10)
N(5)–O(4)–Co(1)	92.1(6)	O(4)–N(5)–O(3)	117.3(8)
O(5)–N(5)–O(4)	120.1(11)		
Dmphen ligand			
N(2)–C(8)	1.323(9)	C(11)–C(29)	1.421(10)
N(2)–C(20)	1.369(9)	C(12)–C(13)	1.348(11)
N(3)–C(17)	1.341(8)	C(13)–C(14)	1.436(11)
N(3)–C(19)	1.373(9)	C(14)–C(15)	1.389(11)
C(7)–C(8)	1.506(12)	C(14)–C(19)	1.406(10)
C(8)–C(9)	1.410(12)	C(15)–C(16)	1.371(11)
C(9)–C(10)	1.335(12)	C(16)–C(17)	1.394(10)
C(10)–C(11)	1.394(12)	C(17)–C(18)	1.498(10)
C(11)–C(12)	1.421(12)	C(19)–C(20)	1.423(10)
C(6)–N(1)–Co(1)	170.2(6)	C(8)–N(2)–C(20)	118.3(6)
C(8)–N(2)–Co(1)	129.1(5)	C(15)–C(14)–C(19)	118.4(7)
C(20)–N(2)–Co(1)	112.6(4)	C(15)–C(14)–C(13)	123.1(7)
C(17)–N(3)–C(19)	118.1(6)	C(19)–C(14)–C(13)	118.5(7)
C(17)–N(3)–Co(1)	128.1(5)	C(16)–C(15)–C(14)	119.1(7)
C(19)–N(3)–Co(19)	113.7(4)	C(15)–C(16)–C(17)	120.3(8)
N(2)–C(8)–C(9)	120.9(8)	N(3)–C(17)–C(16)	122.0(7)
N(2)–C(8)–C(7)	117.2(7)	N(3)–C(17)–C(18)	117.5(6)
C(9)–C(8)–C(7)	121.9(8)	C(16)–C(17)–C(18)	120.5(7)
C(10)–C(9)–C(8)	121.2(8)	N(3)–C(19)–C(14)	122.0(7)
C(9)–C(10)–C(11)	120.5(8)	N(3)–C(19)–C(20)	117.3(6)
C(10)–C(11)–C(12)	125.3(8)	C(14)–C(19)–C(20)	120.6(7)
C(10)–C(11)–C(20)	115.9(8)	N(2)–C(20)–C(21)	123.2(7)
C(12)–C(11)–C(20)	118.8(8)	N(2)–C(20)–C(19)	117.5(6)
C(13)–C(12)–C(11)	121.7(7)	C(11)–C(20)–C(19)	119.4(7)
C(12)–C(13)–C(14)	121.0(8)		

D	A	D···A (Å)
Possible hydrogen bonds[b]		
O(8)	O(5)	2.95(2)
O(8)	O(5c)	3.23(2)

[a] Estimated standard deviations in the last significant digits are given in parentheses. Symmetry transformations: (a) $-x$, $1-y$, $1-z$; (b) $2-x$, $2-y$, $2-z$; (c) $1-x$, $1-y$, $2-z$.

[b] A = acceptor, D = donor.

$(H_2O)_2\}]^+$ (Figs. 1 and 2) mononuclear counterions *trans*-$[Ru(acac)_2(CN)_2]^-$ (Fig. 3) and crystallization water molecules, which are held together by hydrogen bonds and van der Waals forces. The cationic chains are made up by centrosymmetric $[Ni_2(L)(H_2O)_2]^{2+}$ dinuclear motifs connected through the two cyanide groups in *trans* position of the $\{Ru(acac)_2(CN)_2\}^-$ units, affording bimetallic Ru^{III}–Ni^{II}–Ni^{II}–Ru^{III} chains which run along the *b*-axis.

Disregarding the sp^3 hybridized carbon atoms, the remaining part of the macrocyclic ligand *L* is almost planar (maximum atomic deviation 0.13 Å), and encloses two distorted octahedral nickel(II) centers, bridged by phenoxide oxygen atoms. Each nickel atom has two imine–nitrogen [N(1), N(2a) at Ni(1) and N(2), N(1a) at Ni(1a)] and two phenoxide–oxygen [O(1) and O(1a)] atoms forming the strictly planar N_2O_2 equatorial

Table 4
Selected bond lengths (Å) and angles (°)[a] for **3**

Nickel coordination sphere			
Ni(1)–N(1)	2.025(7)	Ni(1)–N(2)	2.087(7)
Ni(1)–N(4)	2.053(7)	Ni(1)–O(4)	2.153(7)
Ni(1)–N(3)	2.061(6)	Ni(1)–O(3)	2.196(7)
N(1)–Ni(1)–N(4)	173.6(3)	N(3)–Ni(1)–O(4)	108.9(2)
N(1)–Ni(1)–N(3)	93.3(3)	N(2)–Ni(1)–O(4)	169.5(3)
N(4)–Ni(1)–N(3)	91.1(2)	N(1)–Ni(1)–O(3)	89.9(3)
N(1)–Ni(1)–N(2)	94.1(3)	N(4)–Ni(1)–N(3)	84.9(3)
N(4)–Ni(1)–N(2)	91.2(3)	N(3)–Ni(1)–O(3)	167.2(3)
N(3)–Ni(1)–N(2)	80.4(3)	N(2)–Ni(1)–O(3)	111.7(3)
N(1)–Ni(1)–O(4)	90.1(3)	O(4)–Ni(1)–O(3)	58.6(3)
Ruthenium coordination sphere			
Ru(1)–O(2)	2.005(5)	Ru(2)–O(7)	1.993(6)
Ru(1)–O(1)	2.002(6)	Ru(2)–O(6)	2.007(5)
Ru(1)–C(6)	2.101(9)	Ru(2)–C(21)	2.063(9)
O(2)–Ru(1)–O(2a)	180.0(1)	O(7b)–Ru(2)–O(7)	180.0(3)
O(2)–Ru(1)–O(1)	89.3(2)	O(7)–Ru(2)–O(6b)	89.1(2)
O(2a)–Ru(1)–O(1)	90.7(2)	O(7)–Ru(2)–O(6)	90.9(2)
O(1)–Ru(1)–O(1a)	180.0(3)	O(6b)–Ru(2)–O(6)	180.0(2)
O(2)–Ru(1)–C(6)	89.7(3)	O(7)–Ru(2)–C(21b)	86.2(3)
O(2b)–Ru(1)–C(6)	90.3(2)	O(6)–Ru(2)–C(21b)	85.9(3)
O(1)–Ru(1)–C(6)	92.9(3)	O(7)–Ru(2)–C(21)	93.6(3)
O(1)–Ru(1)–C(6a)	87.1(3)	O(6)–Ru(2)–C(21)	94.1(3)
C(6)–Ru(1)–C(6a)	180.0(1)	C(21b)–Ru(2)–C(21)	180.0(3)
Cyano groups			
N(1)–C(6)	1.130(10)	N(4)–C(21)	1.138(10)
C(6)–N(1)–Ni(1)	170.1(7)	C(21)–N(4)–Ni(1)	176.8(7)
N(1)–C(6)–Ru(1)	172.9(7)	N(4)–C(21)–Ru(2)	172.4(8)
Acac ligands			
O(1)–C(2)	1.288(11)	O(6)–C(23)	1.272(11)
O(2)–C(4)	1.260(11)	O(7)–C(25)	1.285(11)
C(1)–C(2)	1.517(15)	C(22)–C(23)	1.507(12)
C(2)–C(3)	1.381(13)	C(23)–C(24)	1.386(14)
C(3)–C(4)	1.365(14)	C(24)–C(25)	1.388(13)
C(4)–C(5)	1.515(12)	C(25)–C(26)	1.515(14)
C(2)–O(1)–Ru(1)	119.6(6)	C(23)–O(6)–Ru(2)	122.6(6)
C(4)–O(2)–Ru(1)	123.0(6)	C(25)–O(7)–Ru(2)	122.6(6)
O(1)–C(2)–C(3)	125.5(9)	O(6)–C(23)–C(24)	124.5(8)
O(1)–C(2)–C(1)	112.7(9)	O(6)–C(23)–C(19)	114.8(9)
C(3)–C(2)–C(1)	1201.8(10)	C(24)–C(23)–C(22)	120.7(10)
C(2)–C(3)–C(4)	126.6(9)	C(25)–C(24)–C(23)	127.2(10)
O(2)–C(4)–C(3)	125.0(8)	O(7)–C(25)–C(24)	124.3(8)
O(2)–C(4)–C(5)	114.3(9)	O(7)–C(25)–C(26)	112.1(9)
C(3)–C(4)–C(5)	120.7(9)	C(24)–C(25)–C(26)	123.6(9)
Nitrato ligand			
O(3)–N(5)	1.236(11)	O(5)–N(5)	1.236(12)
O(4)–N(5)	1.262(11)		
N(5)–O(3)–Co(1)	91.0(6)	O(5)–N(5)–O(3)	121.8(11)
N(5)–O(4)–Co(1)	92.2(6)	O(4)–N(5)–O(3)	117.0(10)
O(5)–N(5)–O(4)	121.1(11)		
Dmphen ligand			
N(2)–C(8)	1.328(10)	C(11)–C(29)	1.414(12)
N(2)–C(20)	1.389(10)	C(12)–C(13)	1.339(13)
N(3)–C(17)	1.342(9)	C(13)–C(14)	1.445(13)
N(3)–C(19)	1.386(10)	C(14)–C(15)	1.361(12)
C(7)–C(8)	1.523(14)	C(14)–C(19)	1.443(12)
C(8)–C(9)	1.438(14)	C(15)–C(16)	1.364(13)
C(9)–C(10)	1.354(14)	C(16)–C(17)	1.420(12)
C(10)–C(11)	1.402(13)	C(17)–C(18)	1.482(12)
C(11)–C(12)	1.421(14)	C(19)–C(20)	1.398(11)
C(6)–N(1)–Ni(1)	170.1(7)	C(8)–N(2)–C(20)	118.5(8)
C(8)–N(2)–Ni(1)	129.4(6)	C(15)–C(14)–C(19)	118.8(9)
C(20)–N(2)–Ni(1)	112.0(5)	C(15)–C(14)–C(13)	123.9(9)

Table 4 (*Continued*)

C(17)–N(3)–C(19)	118.6(7)	C(19)–C(14)–C(13)	117.3(9)
C(17)–N(3)–Ni(1)	128.9(5)	C(16)–C(15)–C(14)	120.0(8)
C(19)–N(3)–Ni(1)	112.4(5)	C(15)–C(16)–C(17)	120.3(8)
N(2)–C(8)–C(9)	120.0(9)	N(3)–C(17)–C(16)	121.1(8)
N(2)–C(8)–C(7)	117.5(9)	N(3)–C(17)–C(18)	116.6(7)
C(9)–C(8)–C(7)	122.4(9)	C(16)–C(17)–C(18)	122.2(8)
C(10)–C(9)–C(8)	121.3(9)	N(3)–C(19)–C(14)	120.8(8)
C(9)–C(10)–C(11)	120.1(9)	N(3)–C(19)–C(20)	118.0(7)
C(10)–C(11)–C(12)	124.8(9)	C(14)–C(19)–C(20)	121.2(8)
C(10)–C(11)–C(20)	116.4(9)	N(2)–C(20)–C(21)	123.5(8)
C(12)–C(11)–C(20)	118.7(9)	N(2)–C(20)–C(19)	117.0(7)
C(13)–C(12)–C(11)	122.9(9)	C(11)–C(20)–C(19)	119.5(8)
C(12)–C(13)–C(14)	121.4(9)		

D	A	D···A (Å)
Possible hydrogen bonds[b]		
O(8)	O(5)	3.11(3)
O(8)	O(5c)	3.24(3)

[a] Estimated standard deviations in the last significant digits are given in parentheses. Symmetry transformations: (a) $-x$, $1-y$, $1-z$; (b) $2-x$, $2-y$, $2-z$; (c) $1-x$, $1-y$, $2-z$.

[b] A = acceptor, D = donor.

donor set [maximum atomic deviation 0.020 Å] whereas a water molecule [O(2)] and a cyanide–nitrogen [N(3)] fill the axial positions. The nickel atom is shifted by 0.078 Å from the N_2O_2 basal plane in the direction of the axial cyano ligand. An inversion center is located the middle of Ni_2O_2 plane. The two nickel atoms are separated by 3.1320(6) Å with a Ni(1a)–O(1)–Ni(1) bridge angle of 100.93(7)°, values which compare well with those observed in the ionic salt $[Ni_2(L)(H_2O)_4][Cr(bipy)(ox)_2]_2\cdot H_2O$ (bipy = 2,2′-bipyridine and ox = oxalate dianion) [3.117 Å and 100.28(6)°] [77] and in the tetranuclear complex $[\{M^{III}(phen)(CN)_4\}_2\{Ni_2(L)(H_2O)_2\}]\cdot 2CH_3CN$ (M = Fe and Cr; phen = 1,10-phenanthroline) [3.098(2) Å and 99.66(9)° for M = Fe and 3.101(1) Å and 99.69(11)° for M = Cr] [78].

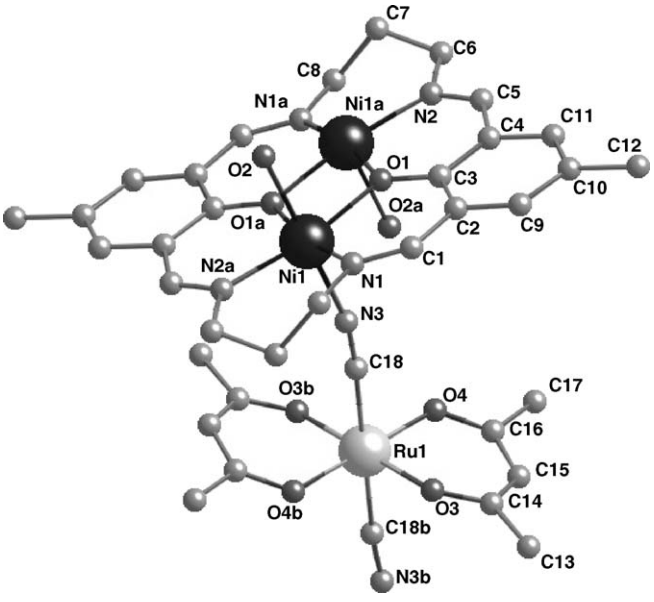

Fig. 1. Perspective drawing of the building block of the cationic chain $[\{Ru(acac)_2(CN)_2\}\{Ni_2(L)(H_2O)_2\}]^+$ (**1**) showing the atom numbering. Hydrogen atoms were omitted for simplicity. Symmetry codes: (a) $-x$, $1-y$, $-z$; (b) $-x$, $-y$, $-z$.

Table 5
Selected bond lengths (Å) and angles (°)[a] for **4**

Ruthenium coordination sphere			
Ru(1)–O(11)	1.95(2)	Ru(1)–O(21)	2.09(2)
Ru(1)–O(12)	2.02(2)	Ru(1)–O(22)	2.02(2)
Ru(1)–C(1)	2.026(13)	Ru(1)–C(2A)	2.048(11)
O(11)–Ru(1)–O(12)	93.0(8)	O(21)–Ru(1)–O(22)	87.9(7)
O(11)–Ru(1)–O(21)	176.2(7)	O(12)–Ru(1)–O(21)	84.6(7)
O(11)–Ru(1)–O(22)	94.5(8)	O(12)–Ru(1)–O(22)	172.4(7)
O(11)–Ru(1)–C(1)	94.8(6)	O(21)–Ru(1)–C(1)	87.8(6)
O(12)–Ru(1)–C(1)	83.7(6)	O(22)–Ru(1)–C(1)	94.7(6)
O(11)–Ru(1)–C(2a)	85.7(6)	O(21)–Ru(1)–C(2a)	91.4(5)
O(12)–Ru(1)–C(2a)	91.4(6)	O(22)–Ru(1)–C(2a)	90.1(5)
C(1)–Ru(1)–C(2a)	175.1(5)		
Ru(2)–O(31)	2.08(2)	Ru(2)–O(41)	1.94(2)
Ru(2)–O(32)	2.04(2)	Ru(2)–O(42)	1.96(2)
Ru(2)–C(1)	2.026(13)	Ru(2)–C(2a)	2.048(11)
O(31)–Ru(2)–O(32)	86.3(8)	O(41)–Ru(2)–O(42)	91.4(9)
O(31)–Ru(2)–O(41)	175.6(8)	O(32)–Ru(2)–O(41)	90.6(9)
O(31)–Ru(2)–O(42)	91.7(9)	O(32)–Ru(2)–O(42)	177.9(8)
O(32)–Ru(2)–C(1)	91.2(7)	O(41)–Ru(2)–C(1)	85.4(7)
O(32)–Ru(2)–C(1)	84.2(6)	O(42)–Ru(2)–C(1)	96.4(8)
O(31)–Ru(2)–C(2a)	88.2(6)	O(41)–Ru(2)–C(2a)	95.5(6)
O(32)–Ru(2)–C(2a)	100.6(6)	O(42)–Ru(2)–C(2a)	78.8(8)
C(1)–Ru(2)–C(2a)	175.1(5)		
Cobalt coordination sphere			
Co(1)–N(1)	1.965(11)	Co(1)–N(2b)	1.978(11)
N(1)–Co(1)–N(1b)	118.9(6)	N(2)–Co(1)–N(2b)	119.7(7)
N(1)–Co(1)–N(2)	104.0(4)	N(1)–Co(1)–N(2b)	105.5(5)
Acac ligand[b]			
O(11)–C(12)	1.24(4)	O(12)–C(14)	1.25(3)
C(12)–C(11)	1.49(5)	C(14)–C(15)	1.54(4)
C(12)–C(13)	1.40(4)	C(14)–C(13)	1.49(4)
O(21)–C(22)	1.23(3)	O(22)–C(24)	1.15(2)
C(22)–C(21)	1.56(4)	C(24)–C(25)	1.43(3)
C(22)–C(23)	1.33(3)	C(24)–C(23)	1.47(4)
O(31)–C(32)	1.21(3)	O(32)–C(34)	1.38(3)
C(32)–C(31)	1.57(4)	C(34)–C(35)	1.73(5)
C(32)–C(33)	1.47(4)	C(34)–C(33)	1.16(4)
O(41)–C(42)	1.26(4)	O(42)–C(44)	1.14(4)
C(42)–C(41)	1.64(5)	C(44)–C(45)	1.67(5)
C(42)–C(43)	1.43(4)	C(44)–C(45)	1.52(5)

[a] Estimated standard deviations in the last significant digits are given in parentheses. Symmetry transformations: (a) $x+1/2$, $-y+3/2$, $z+1/2$; (b) $-x-1$, $-y+1$, $z-1$.

[b] The acac groups are disordered over two sites with 0.64:0.46 occupancies.

Two crystallographically independent ruthenium-containing units [Ru(1) and Ru(2)] occur in **1**, one remaining isolated [Ru(2)] and the other acting as a bismonodentate ligand [Ru(1)] towards the $[Ni_2(L)(H_2O)_2]^{2+}$ unit through its two *trans* coordinated cyanide peripheral groups. This leads to the unprecedented cyano-bridged heterometallic-Ru^{III}–Ni^{II}_2–Ru^{III}-chains. The Ru atoms of both the cationic chain and the free anion have an elongated octahedral coordination, with four acac oxygen atoms defining the equatorial plane [Ru–O bond distances ranging from 2.000(2) to 2.007(2) Å] and two cyanide–carbon atoms occupying the axial positions [Ru–C(cyano) = 2.066(3) Å in the two ruthenium units]. As the ruthenium atoms are situated at centers of symmetry, their equatorial planes show no deviation from

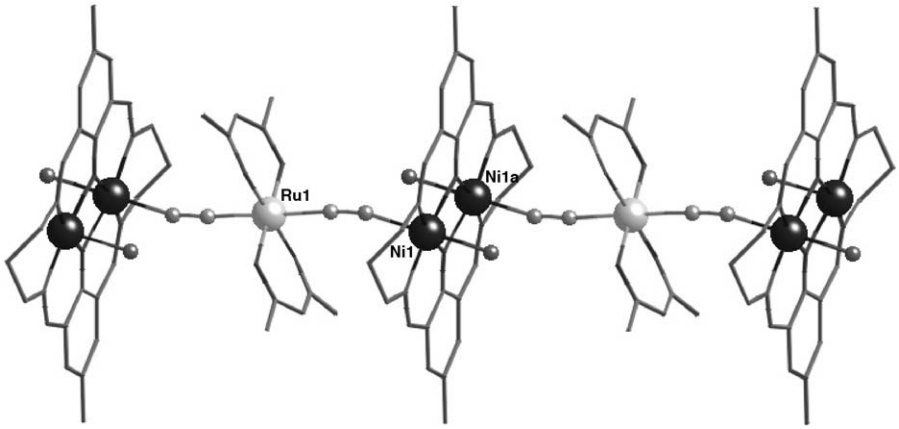

Fig. 2. A view of the cationic chain in **1** along the *b*-axis. Hydrogen atoms were omitted for simplicity.

planarity. The values of the cyanide C–N bonds at Ru(1) are 1.146(3) (in the cationic chain) and 1.142(4) Å (in the anionic unit). The Ru–C–N angles are almost linear: 174.3(2)° (in the chain) and 178.0(3)° (for the counteranion). The Ni(1)–N–C unit at the bridging cyanide is significantly bent 166.4(2)°. The dihedral angle between the equatorial planes of Ni(1) and Ru(1) in the cationic chain is 22.9°. The Ni···Ru distance across the cyano bridge in the cationic chain is 5.2491(5) Å.

The bond distances and angles for the macrocyclic ligand *L* in **1** are in agreement with those observed for this ligand in its homodinuclear metal complexes with nickel(II) [77,78], copper(II) [79–83], cobalt(II) [84] and iron(II) [85] ions.

A view of the crystal packing (Fig. S1) reveals that the anions are situated within the channels created by the parallel cationic chains. In addition to the ionic forces, hydrogen bonds between coordinated water in the cation and the anion cyano groups, stabilize the supramolecular arrangement (see end of Table 2). The coordinated water molecule also participates in hydrogen bonding within the chain. Although hydrogen atoms could not be located on the crystallization water, interatomic distances show that it likely forms hydrogen bonds to cation coordinated water and to an acac oxygen atom of the anion. The shortest metal–metal distance between the cationic chain and anion occurs between nickel and ruthenium linked via a hydrogen bond involving the coordinated water and the cyano nitrogen [6.8543(5) Å for Ni(1)···Ru(2*d*); (*d*) = *x*, *y*, *z* − 1].

3.2. Crystal structure of **2** and **3**

The structure of complexes **2** and **3** is made up of neutral bimetallic chains $[\{Ru^{III}(acac)_2(CN)_2\}\{M^{II}(dmphen)(NO_3)\}]$ [M=Co (**2**) and Ni (**3**)] and crystallization water molecules. The building block and asymmetric unit of this structure is shown in Fig. 4. The two crystallographically independent ruthenium atoms [Ru(1) and Ru(2)] are situated at centers of symmetry, and the chain structure with regular alternating M(II) and Ru(III) ions bridged by single cyano groups, is revealed through application of these symmetry operations (Fig. 5). Each ruthenium atom has elongated octahedral surroundings, four acac–oxygen atoms constituting the equatorial plane [Ru–O ranging from 2.003(4) to 2.013(5) Å and from 1.993(69) to 2.007(5) Å for **2** and **3**, respectively] and the cyanide–carbon atoms occupying the axial positions [Ru–C distances of 2.071(6) and 2.072(8) Å

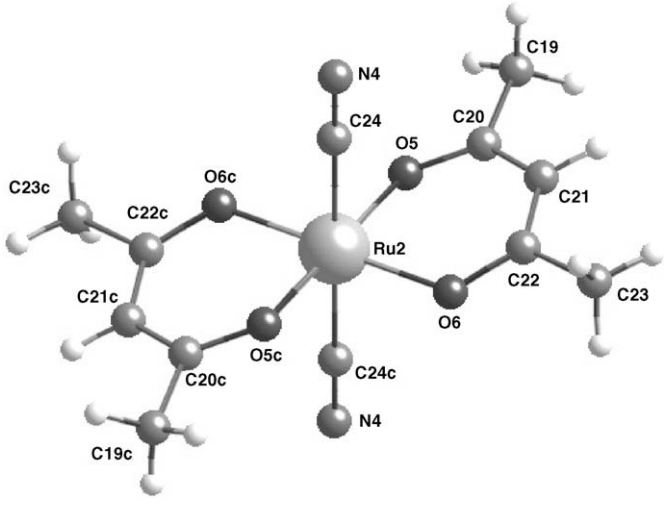

Fig. 3. Perspective drawing of the anion of complex **1** showing the atom numbering. Symmetry code: (c) 1 − *x*, 1 − *y*, 1 − *z*.

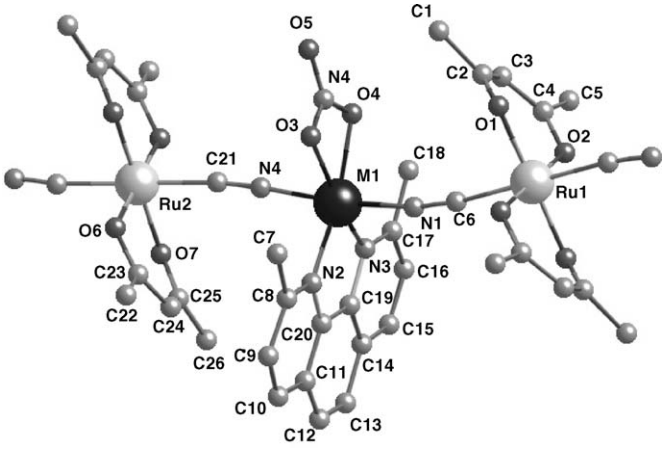

Fig. 4. A view of the asymmetric unit and building block in **2** (M = Co) and **3** (M = Ni) with the atomic numbering scheme. The water molecule and hydrogen atoms were omitted for simplicity.

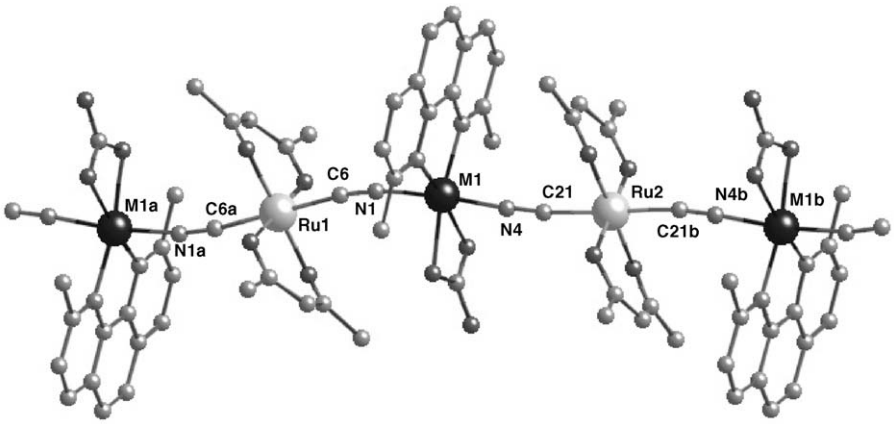

Fig. 5. Fragment of the chain structure of **2** (M = Co) and **3** (M = Ni) running parallel to the *a*-axis. Symmetry codes: (a) $-x, 1-y, 1-z$; (b) $2-x, 2-y, 2-z$.

for **2** and of 2.101(9) and 2.063(9) Å for **3**]. The M atom displays a compressed *cis*-distorted octahedral coordination geometry, binding to bidentate dmphen and nitrate groups in the equatorial plane [M–N of 2.136(6) and 2.100(5) Å (M = Co) and 2.061(6) and 2.087(7) Å (M = Ni); M–O of 2.220(6) and 2.203(6) Å (M = Co) and 2.153(7) and 2.196(7) Å (M = Ni)], and to cyanide–nitrogen atoms in the axial positions [2.050(6) and 2.058(5) Å for Co–N and 2.025(7) and 2.053(7) Å for Ni–N]. The chelating nitrato ligand results in an appreciable distortion of the bond angles in the equatorial plane as the O(3)–M(1)–O(4) angle is only 59.0(2)° (**2**) and 58.6(3)° (**3**). The dmphen ligand is planar and its bond lengths and angles are in agreement with those reported for the free molecule [86,87]. The values of the angle subtended by the dmphen ligand at the cobalt(II) [78.76(2)° for N(2)–Co(1)–N(3)] and nickel(II) [80.4(3)° for N(2)–Ni(1)–N(3)] ions also agrees with those observed in other structurally characterized dmphen-containing cobalt(II) [88–92] and nickel(II) [88,92–105] complexes. The equatorial plane of each ruthenium atom is exactly planar due to symmetry requirements. The equatorial plane at the M atom is essentially planar [maximum atomic deviation 0.019 (**2**) and 0.011 Å (**3**)] and this atom is displaced by 0.092 (**2**) and 0.073 Å (**3**) from the mean plane in the direction of N(1). The dihedral angles between the equatorial planes of Ru and M atoms in the chain are 21.0 (**2**) and 21.4(2)° (**3**) [Ru(1)] and 12.8 (**2**) and 13.0(2)° (**3**) [Ru(2)]. The intrachain M···Ru distances are 5.2038(12) and 5.2426(12) Å for **2** and 5.2130(12) and 5.2353(12) Å for **3**.

Parallel neighboring chains in the crystals are loosely linked into sheets through hydrogen bonds between coordinated nitrate and crystal water (Fig. S2 and end of Tables 3 and 4), and through a slight π–π overlap between dmphen ligands (interplanar distance 3.45 Å), the two types of interactions alternating along the chains.

3.3. Crystal structure of *4*

The structure of **4** consists of two-fold interpenetrated (6,4) three-dimensional networks build up from *trans*-$[Ru^{III}(acac)_2(CN)_2]^-$ anions and Co(II) cations where each cobalt atom is tetrahedrally coordinated by four $[Ru^{III}(acac)_2(CN)_2]^-$ units through the cyano-nitrogen atoms (Fig. 6). In a recent report [45], the reaction of this ruthenium building block with manganese(II) ions in methanol afforded the three-dimensional polymer of formula $\{Mn[Ru(acac)_2(CN)_2]\}_n$ where the manganese atoms have the same environment than that of the cobalt ones in **4** but the resulting structure is a diamond-like one.

The two crystallographically independent ruthenium atoms [Ru(1) and Ru(2)] exhibit a slightly distorted octahedral environment [see Fig. 7 for Ru(1)]. A high standard deviation at the Ru–O(acac) bond distances is observed due to the disorder of the acac groups. This feature does not allow us to determine if the polyhedra around the ruthenium atoms are elongated or compressed. Four planar acac–oxygen atoms build the equatorial plane around the ruthenium atoms, the Ru–O bond distances ranging from 1.95(2) to 2.09(2) Å. These values agree with those observed in the low-spin *trans*-$Ph_4P[Ru(acac)_2(CN)_2]$ [Ru–O = 1.98(2)–2.03(2) Å] [45] and *trans*-$Ph_4As[Ru(acac)_2Cl_2]$ (Ph_4As^+ = tetraphenylarsonium) [Ru–O = 2.010(3)–2.016(3) Å] [46] mononuclear species as well as in the three-dimensional compound $\{Mn[Ru(acac)_2(CN)_2]\}_n$ [Ru–O = 1.995(3) and 2.001(3) Å] [45]. The maximum atomic deviation from the mean equatorial plane in **4** is 0.04(2) Å. Two cyano–carbon atoms fill the apical positions, the Ru–C bond distances

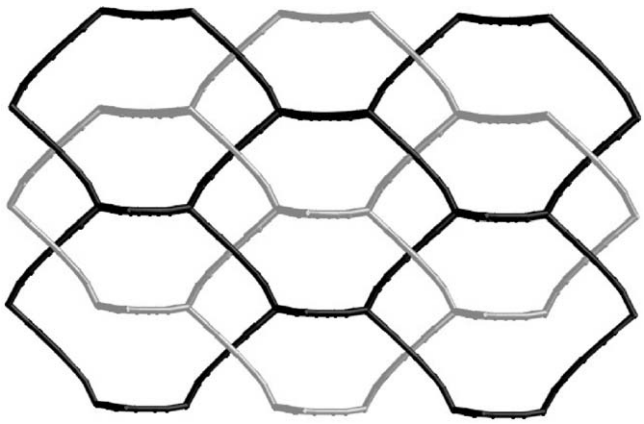

Fig. 6. Projection along the [110] direction of a fragment the two-fold interpenetrated (6,4) three-dimensional Ru^{III}–Co^{II} network in **4**. The edges correspond to Co–Ru–Co motifs whereas the vertexes are occupied by the cobalt atoms.

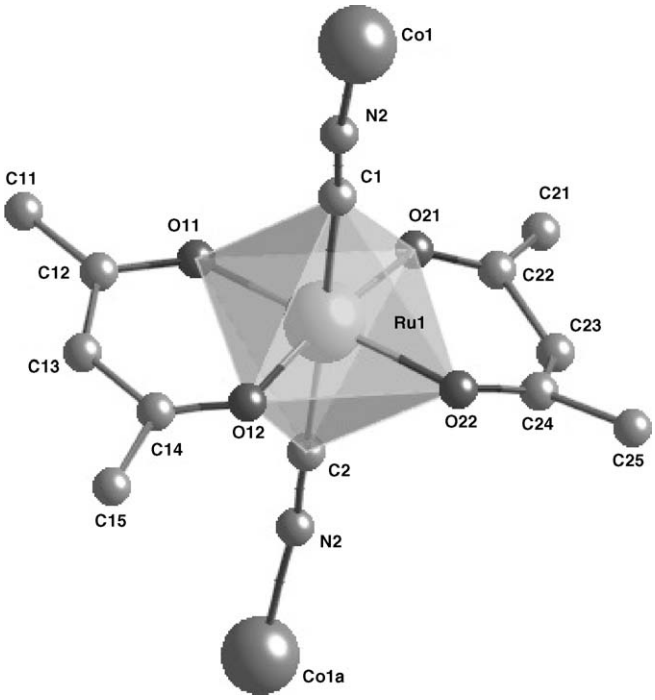

Fig. 7. Perspective view along the [110] direction of the environment of the Ru(1) atom in **4** with the atom numbering.

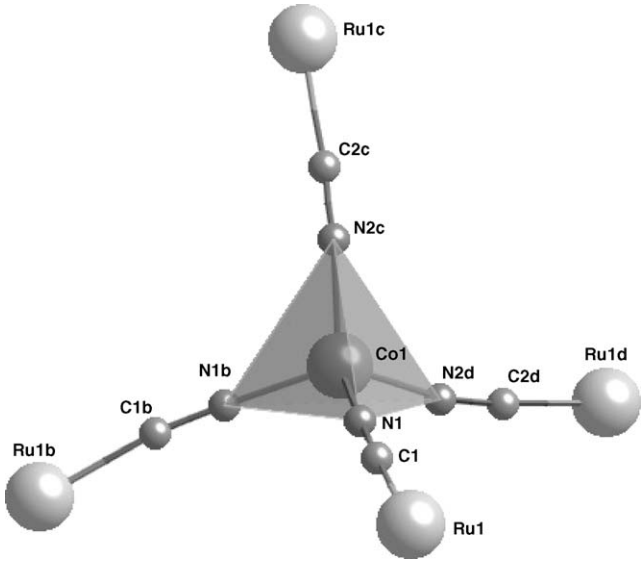

Fig. 8. Perspective view of the environment of the cobalt atom in **4** with the atom numbering.

varying in the range 2.026(11)–2.048(13) Å. The ruthenium atom is shifted by 0.0134(8) Å from the mean equatorial plane towards the C(1) carbon atom. The values of the Ru–C bonds in **4** are very close to those observed in the low-spin *trans*-$Ph_4P[Ru(acac)_2(CN)_2]$ [Ru–C = 2.06(3) and 2.09(3) Å] [45] and $(Ph_4As)_3[Ru(CN)_6]$ [Ru–C = 2.023–2.066 Å] [42] mononuclear complexes.

Each cobalt atom is placed on a two-fold axis and it is surrounded by four cyano-nitrogen atoms [the Co–N bond distances being 1.965(11) and 1.968(11) Å] which define a somewhat distorted tetrahedral environment (see Fig. 8). The maximum deviation of the N–Co–N bond angle from the ideal tetrahedron corresponds to 104.0(4)° for N(1)–Co(1)–N(2). The Co–N bond lengths in **4** are shorter than the Mn–N bond distances observed in the related $\{Mn[Ru(acac)_2(CN)_2]\}_n$ compound [Mn–N = 2.076(3) Å] [45], as expected due the decrease of the ionic radii when going from Mn(II) to Co(II).

Four crystallographically independent acac groups with 0.64 and 0.46 occupancies are present in **4** due to the twinned nature of the crystals. Each acac group chelates the ruthenium atom through its oxygen atoms, forming thus six-membered rings which exhibit slightly distorted envelop conformations. The values of the angle subtended at the metal atom by the acac groups are 93.0(8)° [O(11)–Ru(1)–O(12)], 87.9(7)° [O(21)–Ru(1)–O(22)], 86.3(8)° [O(31)–Ru(1)–O(32)] and 91.4(9)° [O(41)–Ru(1)–O(42)].

The mononuclear cyano-containing $[Ru(acac)_2(CN)_2]^-$ units act as bis-monodentate ligands towards the cobalt(II) cations through its two *trans*-coordinated cyano groups, affording twelve gon cycles which are constituted by six ruthenium and six cobalt atoms with regular alternating of cobalt and ruthenium atoms (see Fig. 9a). The C(1)–N(1) and C(2)–N(2) bond distances are 1.134(14) and 1.124(14) Å [to be compared with the values of 1.12(3) and 1.15(3) Å in the mononuclear *trans*-$Ph_4P[Ru(acac)(CN)_2]$ complex]. The Ru–C–N and Co–C–N bond angles are quite linear: 176.7(11)° and 172.2(10)° [at Ru(1)] and 170.0(11)° and 173.2(11)° [at Co(1)]. The values of the distance between adjacent ruthenium and cobalt atoms within the ten gon cycle are 5.1155(15) and 5.1100(15) Å for Ru(1)···Co(1) and Ru(1)···Co(1a), respectively [symmetry code: (a) $x + 1/2, -y + 3/2, z + 1/2$].

Each cobalt atom is cyano-bridged to four ruthenium atoms leading thus to a (6,4) three-dimensional network [see Fig. 9b]. Finally, two three-dimensional networks interpenetrate each other to form the crystal structure of **4** (see Fig. 6).

3.4. Magnetic properties of *1–4*

Although the magnetic properties of the mononuclear complex *trans*-$Ph_4P[Ru(acac)_2(CN)_2]$ were published elsewhere [45], we decided to reinvestigate them in order to analyze properly the magnetic behavior of compounds **1**–**4** where the $[Ru(acac)_2(CN)_2]^-$ unit is present as a ligand (**1**–**4**) and counterion (**2**). The temperature dependence of $\chi_M T$ for the *trans*-$Ph_4P[Ru(acac)_2(CN)_2]$ compound [χ_M is the molar magnetic susceptibility] is shown in Fig. 10. The value of $\chi_M T$ at 270 K is 0.51 $cm^3\ mol^{-1}\ K$ ($\mu_{eff} = 1.96\ \mu_B$) and $\chi_M T$ exhibits a quasi linear dependence with T in the temperature range investigated reaching a value of 0.44 $cm^3\ mol^{-1}\ K$ at 2.0 K. This behavior is the expected one for a low-spin distorted octahedral ruthenium(III) system (t_{2g}^5, $S_{Ru} = \frac{1}{2}$) with spin-orbit coupling of the $^2T_{2g}$ ground term. The low spin nature of this Ru(III) complex is corroborated by the magnetization versus H plot at 2.0 K (see inset of Fig. 10). One can see there how the magnetization increases linearly at low fields and it tends to a saturation value of 1.08 BM at 5 T. The Q-band EPR spectrum of a polycrystalline

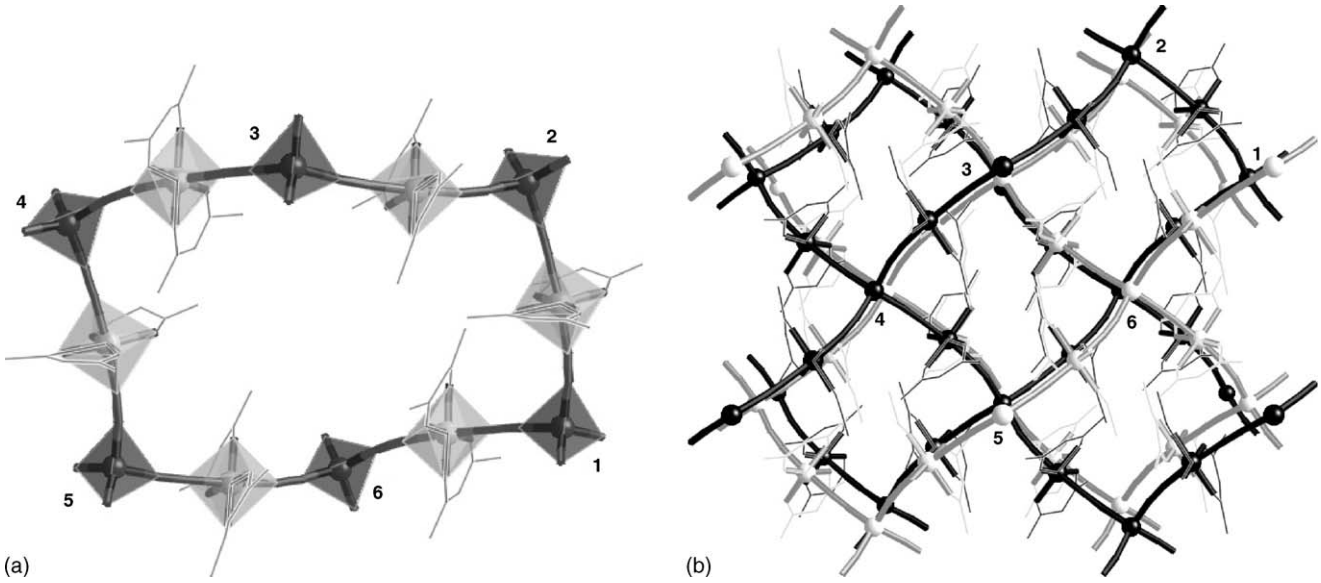

Fig. 9. Perspective view of the twelve gon cycle of **4** in the *bc* plane (a) which forms the (6,4) three-dimensional network (b).

sample of this compound at 67 K (Fig. 11) shows a rhombic pattern with $g_1 = 2.55$, $g_2 = 2.21$ and $g_3 = 1.69$ ($g_{av} = 2.15$). The calculated value for M_{sat} ($M_{sat} = gS = 2.15/2\ \mu_B$) is practically identical to the experimental one ($1.08\ \mu_B$). In order to analyze the magnetic properties of the low-spin complex *trans*-$Ph_4P[Ru(acac)_2(CN)_2]$, one must take into account that its $^2T_{2g}$ ground term in O_h symmetry is split under a rhombic distortion (C_{2v} symmetry) into a singlet low-lying state ($^2A_1$) and two excited doublets ($^2B_1 + {}^2B_2$) which are considered quasi degenerated, in a first approach, and separated by an energy gap, denoted Δ. Having in mind these considerations, we treated the magnetic data of the compound *trans*-$Ph_4P[Ru(acac)_2(CN)_2]$ through a Hamiltonian which takes into account the rhombic distortion, spin-orbit coupling and the Zeeman effect [106]. Best-fit parameters are: $\Delta = 1627(10)$, $\lambda = -1067(5)\ cm^{-1}$ and $k = 0.89(1)$, where λ is the spin-orbit coupling and k is the orbital reduction factor.

The magnetic properties of complex **1** in the form of $\chi_M T$ plot [χ_M is the magnetic susceptibility per $Ni_2^{II}Ru_2^{III}$ unit] are shown in Fig. 12. $\chi_M T$ at 280 K is equal to $3.41\ cm^3\ mol^{-1}\ K$, a value which is as expected for a four spin system made up of two spin triplets ($S_{Ni} = 1$ with g_{Ni} ca. 2.20) and two spin doublets ($S_{Ru} = \frac{1}{2}$ with g_{Ru} ca. 2.15). Upon cooling, $\chi_M T$ continuously decreases, reaches a quasi plateau at 10–8 K [$\chi_M T = 0.85\ cm^3\ mol^{-1}\ K$] and further decreases to a value of $0.66\ cm^3\ mol^{-1}\ K$ at 1.9 K. These features are characteristic of an overall antiferromagnetic behavior. Keeping in mind

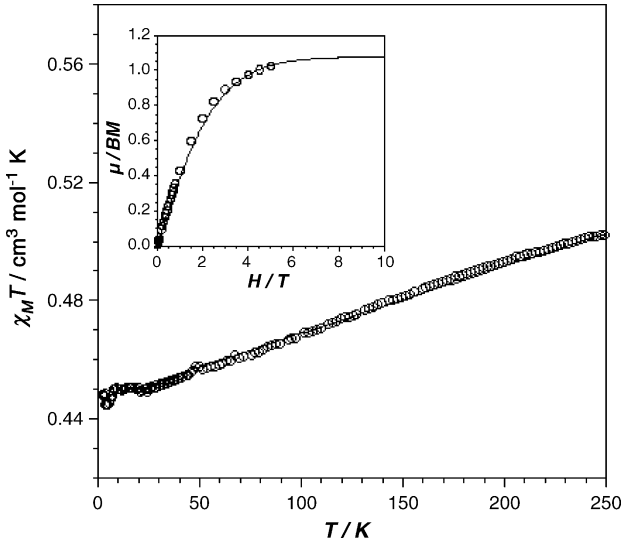

Fig. 10. Thermal dependence of the $\chi_M T$ product for the *trans*-$Ph_4P[Ru(acac)_2(CN)_2]$ mononuclear complex under an applied magnetic field of 1 T: (◯) experimental data; (—) best-fit curve (see text). The inset shows the magnetization vs. H plot at 2.0 K: (◯) experimental data; (—) Brillouin function for a spin doublet with $g = 2.15$.

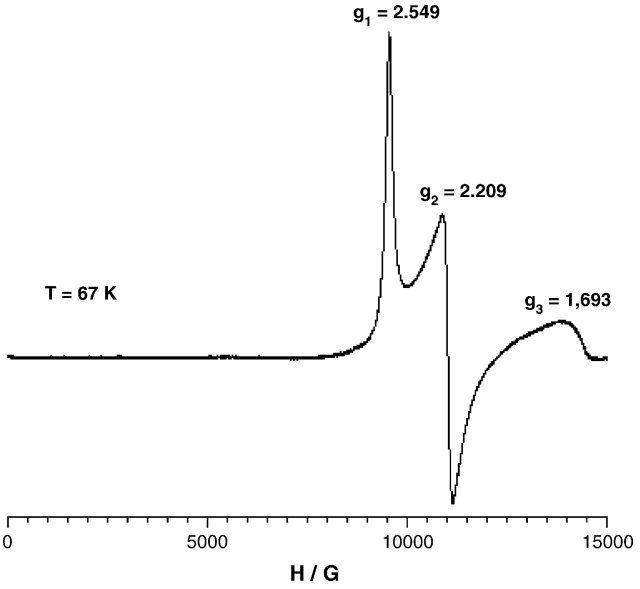

Fig. 11. Q-band EPR spectra of a polycrystalline sample of *trans*-$Ph_4P[Ru(acac)_2(CN)_2]$ at 67 K.

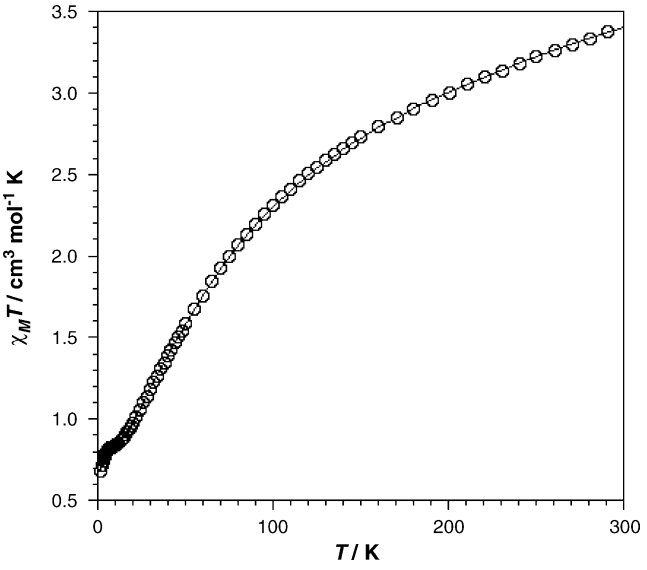

Fig. 12. Thermal dependence of $\chi_M T$ for complex **1** under an applied magnetic field of 1 T: (◯) experimental data; (—) best-fit curve (see text).

the alternating chain structure of **1**, two intrachain exchange pathways are involved: the double phenoxo bridge [between two nickel(II) ions] and the single cyanide bridge [between a nickel(II)–ruthenium(III) pair]. As a strong antiferromagnetic interaction between the nickel(II) ions through the double phenoxo bridge has been demonstrated in previous works [$-J$ values varying in the range 44.4–72 cm^{-1}, the Hamiltonian being defined as $\hat{H} = -J\hat{S}_{\mathrm{Ni}}\,\hat{S}_{\mathrm{Nia}}$] [78,85,107] and a weak ferromagnetic interaction is expected for the Ni(II)–Ru(III) pair through the single cyano bridge (case of strict orthogonality between the interacting magnetic orbitals [e_g (Ni) versus t_{2g} (Ru)], the former interaction would account for the decrease of $\chi_M T$ in Fig. 12 until very low temperatures. The expected intrachain spin topology [relatively strong antiferromagnetic interaction between the nickel(II) ions through the double phenoxo bridge and a weak ferromagnetic coupling between adjacent nickel(II) and ruthenium(III) ions through the single cyano bridge] would lead to a singlet ground spin state ($S = 0$). The presence of the magnetically isolated $[Ru(acac)_2(CN)_2]^-$ unit in **1** accounts for the value of $\chi_M T$ at very low temperatures (ca. 0.45 cm^3 mol^{-1} K). There is no theoretical model to analyze properly the magnetic data of this chain. However, we can calculate the magnetic susceptibility of a Heisenberg linear chain by using a closed-chain computational procedure [108] as a function of the exchange interaction between first neighbors. In this procedure, the infinite chain behavior can be obtained by extrapolation from the exact result for the increasing ring length. In the case of complex **1**, the isotropic exchange Hamiltonian can be written as [Eq. (1)]

$$\hat{H} = -\sum_{i=0}^{N/3-1} J_1 \hat{S}_{3i+1}\hat{S}_{3i+2} - \sum_{i=0}^{N/3-1} J_2(\hat{S}_{3i+2}\hat{S}_{3i+3} + \hat{S}_{3i+3}\hat{S}_{3i+4}) \quad (1)$$

where N is the total number of interacting spins which is limited here to four pairs of triplets and four pairs of doublets and J_1 and J_2 are the exchange coupling parameters associated to the two exchange pathways [one through the double phenoxo group between nickel(II) ions and the other through the single cyano bridge between low-spin ruthenium(III) and nickel(II) ions]. An average Landé factor g was considered for both nickel(II) and low-spin ruthenium(III) ions. A constant $\chi_M T$ term was also introduced to account for the presence of the uncoordinated *trans*-$[Ru(acac)_2(CN)_2]^-$ anion. We have assumed that the $N = 12$ ring is the closer solution to the exact one in the whole experimental temperature range. Due to the exchange topology of the system, it is not possible to find a set of spin quantum numbers for which the eigenmatrix is diagonal. So, there is no analytical expression for the energy values as a function of the exchange parameters and numerical methods are needed to evaluate and diagonalize the eigenmatrix. These calculations were performed with the magnetic package MAGPACK [109,110]. The best-fit parameters were $J_1 = -50.0$ cm^{-1}, $J_2 = +6.6$ cm^{-1} and $g = 2.12$. The calculated curve matches very well the experimental data in the whole temperature range explored (1.9–295 K).

In the light of the available data (see above), it is clear that J_1 (-50.0 cm^{-1}) corresponds to the magnetic coupling between the nickel(II) ions through the double phenoxo group. This value is very close to those observed in the tetranuclear compounds $[\{M^{III}(phen)(CN)_4\}_2\{Ni_2(L)(H_2O)_2\}]\cdot 2CH_3CN$ [M = Fe ($J = -44.4$ cm^{-1}) and Cr ($J = -44.6$ cm^{-1})], this similarity being due to the close values of the nickel–nickel separation through the double phenoxo group [3.1320(6) Å in **1** versus 3.098(2) Å (M = Fe) and 3.101(1) Å (M = Cr)] and the angle at the phenoxo bridge [100.93(7)° in **1** versus 99.66(9)° (M = Fe) and 99.69(11)° (M = Cr)] [78]. J_2 would correspond to the magnetic interaction between adjacent Ni(II) and Ru(III) ions and its ferromagnetic nature is as expected for a strict orthogonality between the interacting magnetic orbitals (see below). To our knowledge, this is the first time that such an interaction has been evaluated and consequently, no comparison can be made.

The magnetic properties of complex **2** in the form of $\chi_M T$ versus T plot [χ_M is the magnetic susceptibility per $Co^{II}Ru^{III}$ unit] are shown in Fig. 13. At room temperature, $\chi_M T$ is equal to 3.15 cm^3 mol^{-1} K, a value which is as expected for a pair of magnetically isolated high-spin cobalt(II) ($S_{Co} = \frac{3}{2}$) and low-spin ruthenium(III) ($S_{Ru} = \frac{1}{2}$) ions with orbitally degenerate $^4T_{1g}$ and $^2T_{2g}$ single ion ground states, respectively. As the temperature is lowered, the $\chi_M T$ product smoothly decreases, exhibits a minimum at 28 K ($\chi_M T$ being 2.99 cm^3 mol^{-1} K), and further increases sharply to reach a value of 11.3 cm^3 mol^{-1} K at 1.9 K. The fact that the value of $\chi_M T$ at the minimum is well above that calculated for a high-spin Co(II) and a low-spin Ru(III) magnetically non-interacting pair, supports the occurrence of an intrachain ferromagnetic interaction between the Co(II) and Ru(III) centers, the smooth decrease of $\chi_M T$ in the high temperature range being due to spin-orbit coupling effects of both metal ions. No magnetic ordering, is observed above 1.9 K showing that the ferromagnetic chains are well isolated from each other.

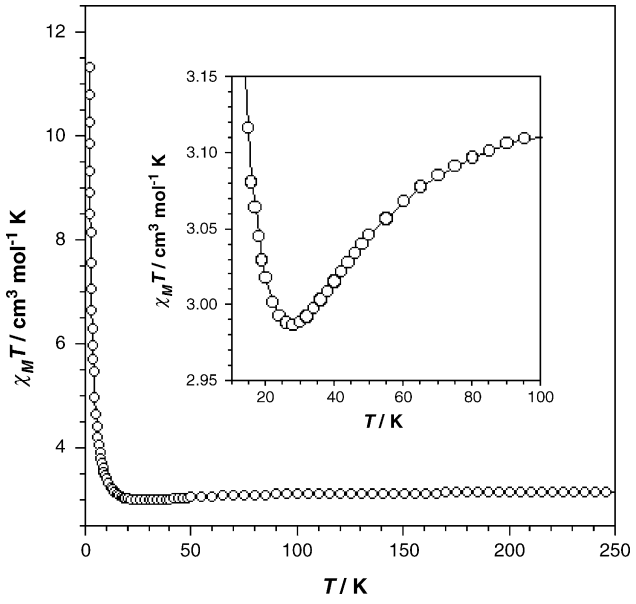

Fig. 13. Thermal dependence of the $\chi_M T$ product for complex **2** under applied magnetic fields of 1 T ($T \geq 50$ K) and 100 G ($T < 50$ K): (◯) experimental data; (—) eye-guide line. The inset shows the $\chi_M T$ plot in the vicinity of the minimum.

The M versus H plot at 2.0 K for **2** (see Fig. 14), M being the magnetization per $Ru^{III}Co^{II}$ unit, confirms the ferromagnetic nature of the intrachain magnetic coupling. The magnetization tends to a saturation value close to 3.07 μ_B at 5 T (the maximum available field in our SQUID). This is consistent with the parallel alignment of two spin doublets, one from the Ru(III) with $g_{Ru} = 2.15$ and the other from the Co(II) with g_{Co} ca. 4.3 [at low temperatures, only the ground Kramers doublet of an octahedral cobalt(II) ion is thermally populated and $g_{Co} = (10 + 2A\kappa)/3$ with values of A and κ of ca. 1.5 and 0.8, respectively] [111]. The intrachain magnetic coupling in **2** cannot be evaluated due to the lack of a suitable model to analyze its magnetic properties. The increasing ring size methodology to mimic a chain that we have used in the case of compound **3** (see below) does not apply in the compound **2** because the problems associated to the occurrence of a significant orbital contribution of the octahedral high-spin cobalt(II) ion which dominates the magnetic behavior of **2** in a wide range of temperature.

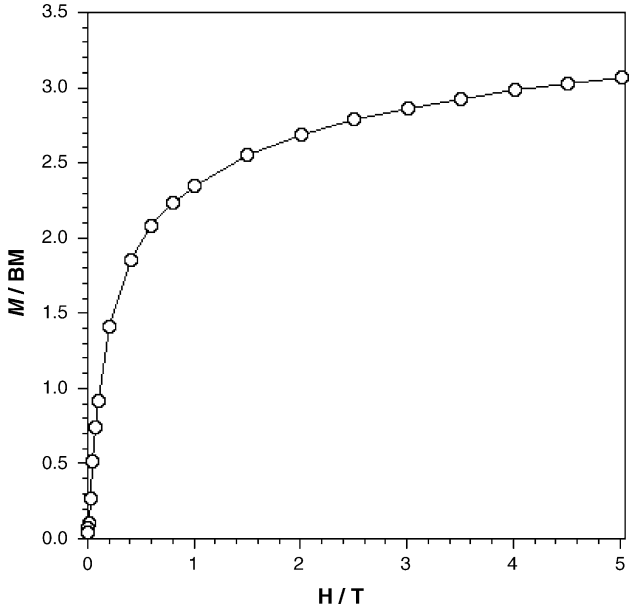

Fig. 14. Magnetization vs. H plot for complex **2** at 2.0 K: (◯) experimental data; (—) eye-guide line.

The magnetic properties of complex **3** in the form of $\chi_M T$ versus T plot [χ_M is the magnetic susceptibility per $Ru^{III}Ni^{II}$ unit] are shown in Fig. 15. The shape of this plot is typical of a ferromagnetic interaction. At room temperature, $\chi_M T$ is equal to 1.60 cm^3 mol^{-1} K, a value which is as expected for a pair of magnetically isolated nickel(II) ($S_{Ni} = 1$) and low-spin ruthenium(III) ($S_{Ru} = \frac{1}{2}$) ions. $\chi_M T$ continuously increases when cooling and reaches a value of 4.10 cm^3 mol^{-1} K at 1.9 K. No magnetic ordering, was observed above 1.9 K showing that the ferromagnetic chains are well isolated from each other, as in **2**. The M versus H plot at 2.0 K for **3** (see inset of Fig. 15), M being the magnetization per $Ru^{III}Ni^{II}$ unit, confirms the ferromagnetic nature of the intrachain magnetic coupling. The magnetization increases sharply at very low fields at it reaches a value of 3.0 μ_B at 5 T (the maximum available field in our SQUID). This value is close to that expected for the parallel alignment of a spin triplet ($S_{Ni} = 1$) and a spin doublet ($S_{Ru} = \frac{1}{2}$). Compound **3** behaves thus as a ferromagnetic chain with regular alternating nickel(II) and ruthenium(III) ions.

In the lack of a theoretical model to analyze the magnetic data of this chain compound, we tried to get a numerical expression by considering closed spin chains of increasing length containing regular alternating of a spin doublet and a spin triplet. The isotropic exchange Hamiltonian may be written as [Eq. (2)]

$$\hat{H} = -\sum_{i=1}^{N-1} J \hat{S}_i \hat{S}_{i+1} \quad (2)$$

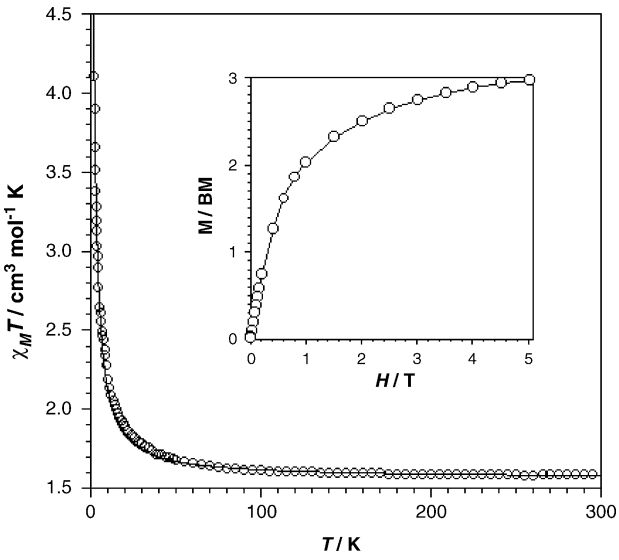

Fig. 15. Thermal dependence of the $\chi_M T$ product for complex **3** under applied magnetic fields of 1 T ($T \geq 50$ K) and 100 G ($T < 50$ K): (◯) experimental data; (—) best-fit curve (see text). The inset shows the: (◯) experimental data; (—) eye-guide line.

The calculations were limited up to $N = 12$ (six pairs of spins $1–\frac{1}{2}$). We have assumed that the $N = 12$ ring is the closer solution to the exact one in the full experimental temperature range. As for **1**, due to the exchange topology of the system, it is not possible to find a set of spin quantum number for which the eigenmatrix is diagonal. So, there is no analytical expression for the energy values as a function of the exchange parameter and we need to use numerical methods to evaluate and diagonalize the eigenmatrix. These calculations were performed with the magnetic package MAGPACK [109,110]. Best-fit values are $J = +3.2\,\mathrm{cm}^{-1}$, $g = 2.20$ and $R = 2.1 \times 10^{-5}$ [R is the agreement factor defined as $R = \sum [(\chi_M T)_{exp}(i) - (\chi_M T)_{calcd}(i)]^2 / \sum [(\chi_M T)_{exp}(i)]^2$]. The calculated curve matches very well the experimental data in the whole temperature range investigated (1.9–295 K). The nature of this magnetic coupling is the same than that observed for the similar cyano-bridged Ru(III)–Ni(II) unit in **1** given that the strict orthogonality between the interacting magnetic orbitals also applies in **3**. The difference in the magnitude of the two ferromagnetic couplings (+6.6 cm^{-1} in **1** versus +3.2 cm^{-1} in **3**) is most likely due to subtle structural differences such as the different chomophore around the nickel atom (NiO_4N_2 in **1** versus NiO_2N_4 in **3**) [112] and the greater distortion of the environment of the nickel atom in **3** due to the coordination of the nitrate group as an asymmetrical bidentate ligand.

The magnetic properties of complex **4** in the form of $\chi_M T$ versus T plot [χ_M is the magnetic susceptibility per $Ru_2^{III}Co^{II}$ unit] are shown in Fig. 16. At room temperature, $\chi_M T$ is equal to 3.70 $\mathrm{cm}^3\,\mathrm{mol}^{-1}\,\mathrm{K}$, a value which is somewhat above that expected for a high-spin tetrahedral Co(II) center and two low-spin Ru(III) ions. $\chi_M T$ continuously increases when cooling from room temperature to 10 K, then exhibits a sharp increase to reach a maximum value of 242 $\mathrm{cm}^3\,\mathrm{mol}^{-1}\,\mathrm{K}$ at 4.5 K and further decreases linearly with T to 120 $\mathrm{cm}^3\,\mathrm{mol}^{-1}\,\mathrm{K}$ at 1.9 K. These features suggest a long-range ferromagnetic ordering. In fact, the field-cooled magnetization (FCM) of **4** under 100 G (inset of Fig. 16) increases abruptly below 6.5 K indicating the onset of a long-range magnetic phase transition with T_c below 6.5 K. The magnetization of **4** at 2.0 K increases rapidly at low fields and reaches a quasi saturation value of 5.0 μ_B at 5 T, which is very close to the expected one for a parallel alignment of the magnetic moments of two low-spin Ru(III) ions and one tetrahedral Co(II) center. A characteristic hysteresis loop of a soft magnet is observed at 2.0 K (see inset of Fig. 17) with values of the remnant magnetization and coercive field of 0.40 μ_B and

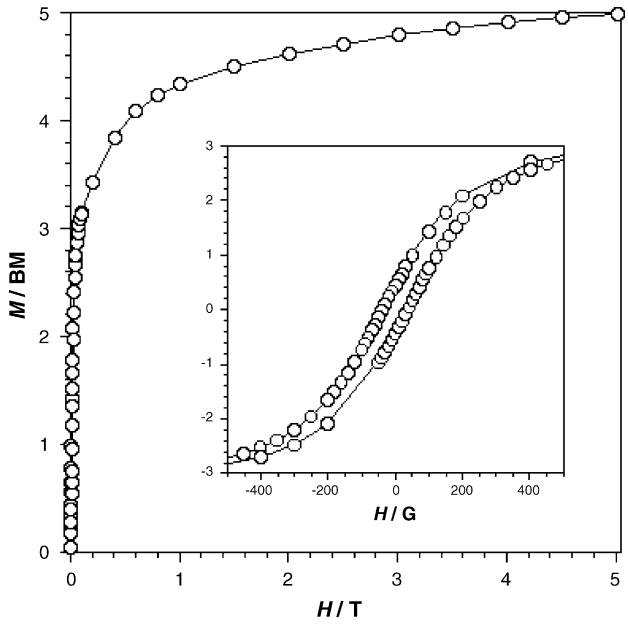

Fig. 17. Magnetization vs. H plot for complex **4** at 2.0 K: (◯) experimental data; (—) eye-guide line. The inset shows the hysteresis loop of complex **4** at 2.0 K.

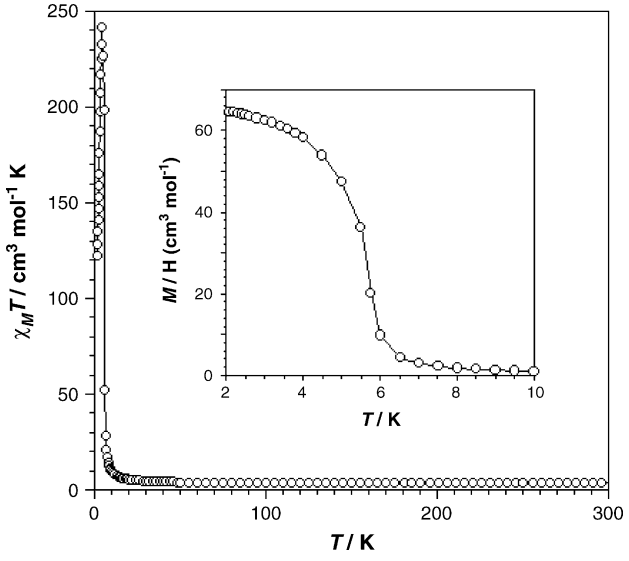

Fig. 16. Thermal dependence of the $\chi_M T$ product for complex **4** under applied magnetic fields of 1 T ($T \geq 50$ K) and 100 G ($T < 50$ K): (◯) experimental data; (—) eye-guide line. The inset shows the FCM plot in the low temperature region at 100 G.

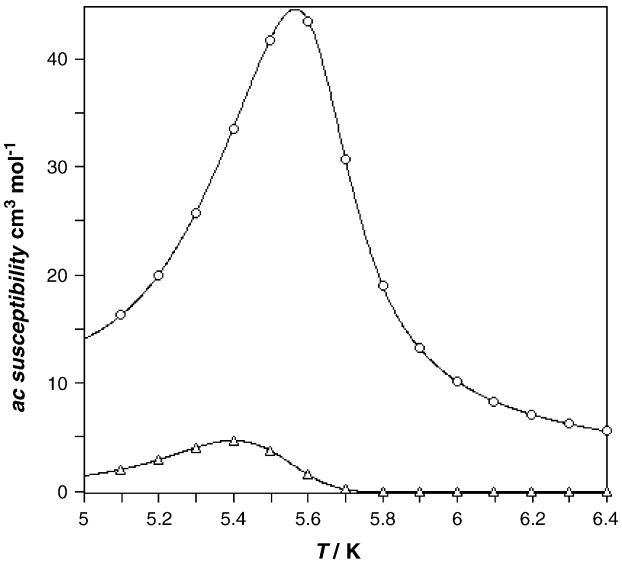

Fig. 18. Thermal dependence of the in-phase (◯) and out-of-phase (△) ac susceptibility signals for **4** in the lack of applied external field and under an oscillating magnetic field of ±1 G and a frequency of 1000 Hz.

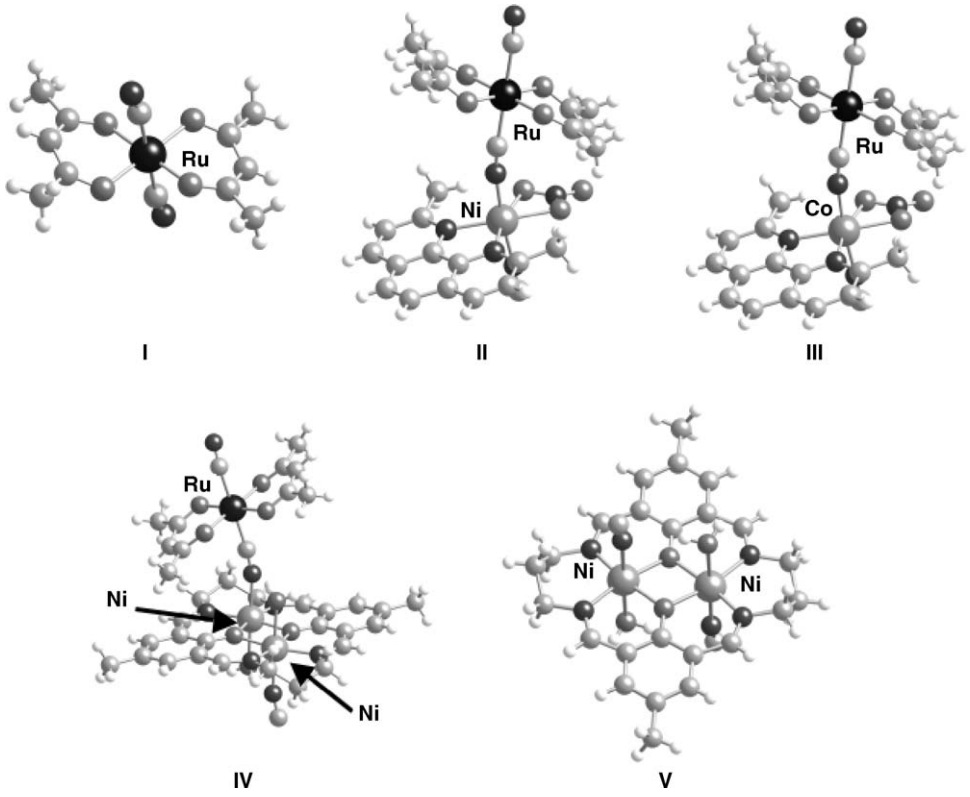

Fig. 19. Mononuclear *trans*-$[Ru(acac)_2(CN)_2]^-$ (**I**), heterodinuclear Ru^{III}–CN–Ni^{II} (**II**) and Ru^{III}–CN–Co^{II} (**III**), heterotrinuclear Ru^{III}–CN–$Ni^{II}O_2Ni^{II}$ (**IV**) and homodinuclear $Ni^{II}O_2Ni^{II}$ (**V**) models used in the DFT calculations concerning compounds **1**–**3**.

30 G, respectively. Finally, the ferromagnetic ordering temperature $T_c = 5.4$ K was further confirmed from the maximum of the out-of-phase ac susceptibility at zero external field (Fig. 18). No significant frequency dependence was observed in the ac measurements of **4**.

3.5. Analysis of the exchange pathways in *1–4*

The models to analyze the exchange interactions in complexes **1**–**3** through DFT type calculations are shown in Fig. 19. Models **IV** and **V** correspond to complex **1**. The analysis of both models allow us to study the influence of the presence of Ru^{III} on the value of the magnetic coupling of the double phenoxo-bridged nickel(II) unit. As indicated in the computational paragraph, we have used a 3-21G basis set for the ruthenium atom. In order to analyze the possible influence of the basis set on the evaluation of the magnetic couplings, we have used different basis sets for the atoms other than ruthenium. The results obtained are listed in Table 6. One can see there that similar results are obtained independently of the basis set used. In most of the cases, a smaller variation in the values of the results is observed through the basis sets proposed by Ahlrichs. Consequently, the use of simpler basis sets (SV) leads to the same quality results than that of more extended ones (TZV). From a qualitative point of view, the results obtained by DFT calculations on the models **III**–**V** agree well with the experimental values, in particular in **IV** and **V** where they can be compared with the *J* values of complex **1**. So, in agreement with the experimental values, an antiferromagnetic interaction between the nickel(II) ions through the double phenoxo-bridge is found which is stronger than the ferromagnetic coupling between the ruthenium(III) and nickel(II) ions through the single cyano bridge in the same com-

Table 6
Calculated values of the magnetic coupling[a] for the models **II**–**V**

Basis set[b]	$J_{Ru–Ni}$ (**II**)	$J_{Ru–Co}$ (**III**)	$J_{Ru–Ni}$ (**IV**)	$J_{Ni–Ni}$ (**IV**)	$J_{Ni–Ni}$ (**V**)
3-21G/3-21G	+107.7	+7.6	+5.2	−27.9	−23.3
6-31G/3-31G	+111.1	+6.4	+3.7	−33.1	−25.7
6-31G/6-31G	+95.6	+6.7	+4.3	−37.9	−25.7
SV/SV	+93.9	+5.6	+3.6	−34.5	−21.3
T7V/SV	+93.7	+5.7	+3.6	−33.6	−18.9
T7V/T7V	+93.2	+5.7	+3.9	−41.4	−32.2

[a] The values of the magnetic coupling are given in cm^{-1}.
[b] The description of the basis sets is given in the paragraph of the computational strategy. The first basis set is that used for the metal atoms other than ruthenium whereas the second one concerns the remaining atoms.

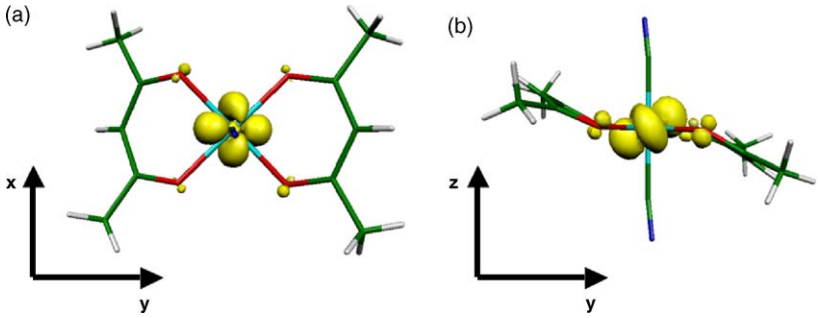

Fig. 20. Spin density map for model **I**. The values of the atomic spin densities in electron units are: +0.86 (Ru), +0.04 (O), −0.02 (C_{cyano}), +0.01 (N_{cyano}). Average values are given for the atoms other than ruthenium. Spin density is plotted with cutoff at 0.010 e.

plex (−41.4 and +3.9 cm^{-1}, respectively). The fact that the calculated values of the $J_{Ni–Ni}$ parameter in **IV** and **V** are similar validates the models chosen. Anyway, the more complete model **IV** provides values of the $J_{Ni–Ni}$ parameter which are closer to the experimental one of complex **1** and those given in Refs. [78,85,107]. This induces us to conclude that a larger fragment of bimetallic chain would provide more accurate values of $J_{Ni–Ni}$.

A weak ferromagnetic interaction is predicted for the magnetic coupling between the ruthenium(III) and the cobalt(II) ions through the single cyano bridge whose value cannot be computed from the experimental data because of the spin-orbit coupling of the octahedral cobalt(II) ion. Anyway, the shape of the $\chi_M T$ versus T plot of **2** in the low temperature range agrees with the occurrence of a weak ferromagnetic interaction. The lack of magneto-structural data concerning this type of cyano-bridged heterometallic unit precludes any comparison with the calculated magnetic coupling by DFT.

The nature of the magnetic coupling (weak ferromagnetic interaction) found between the low-spin ruthenium(III) and either the nickel(II) (**1** and **3**) or cobalt(II) ions (**2**) is as expected taking into account the symmetry of the magnetic orbitals involved (t_{2g} versus e_g type magnetic orbitals). The orientation of the magnetic orbital of the *trans*-$[Ru(acac)_2(CN)_2]^-$ is not the more appropriate to mediate strong magnetic interactions through bridging cyano in **1**–**3**. As shown in Fig. 20, the unpaired electron of this mononuclear unit is roughly located in the equatorial plane defined by the four acetylacetonato-oxygens ($d_{x^2-y^2}$ type orbital), the spin density on the cyano groups (which define the z-axis) being negligible. Having this in mind and under ideal conditions, a very weak ferromagnetic interaction or lack of magnetic coupling can be expected even for complex **4** where the cobalt(II) ion is tetrahedral (half filled t_{2g} orbitals, $e_g^4 t_{2g}^3$). The experimental results and the theoretical calculations on the models **III** and **IV** agree with this prediction. This inappropriate orientation of the magnetic orbital of the low-spin ruthenium(III) unit accounts for the weaker ferromagnetic interaction in the single cyano-bridged Ru(III)–Ni(II) unit [J values of +6.6 (**1**) and +3.2 cm^{-1} (**2**)] when compared to that found in the related single cyano-bridged Fe(III) (low-spin)–Ni(II) entity (J = +17.4 cm^{-1}) [78]. The more favorable orientation of the magnetic orbital in the low-spin $[Fe(phen)(CN)_4]^-$ unit (the magnetic orbital is perpendicular to the mean phen plane) leads to a significant ferromagnetic coupling between the low-spin iron(III) and nickel(II) ions.

However, a relatively strong ferromagnetic interaction is obtained by DFT calculations on the model **II** (see Table 6). At this respect, it deserves to be noted that (i) firstly, the nature of the magnetic interaction is correctly predicted by the calculations and (ii) secondly, several reasons would account for the overestimation of the magnitude of the magnetic coupling. They can be summarized as follows: (a) uncommon difficulties to reach convergence have been found in the present case (model **II**); (b) the quality and reliability of the basis set of the second row transition metal ions are poorer than those of the 3d metal ions; (c) the relativistic effects characteristic of the heavier elements may be present in the ruthenium atom; (d) finally, the overestimation of the magnitude of the exchange coupling by DFT calculations in other cyano-bridged polynuclear systems has been noted by us previously [78,113,114]. In an attempt to overcome this problem, a possible solution for a near future would be to consider more extended models and also to introduce the solid effects by a dielectric medium.

4. Conclusions

We have shown how the use of the building block *trans*-dicyanobis(acetylacetonato)ruthenate(III) as a ligand towards coordinatively unsaturated preformed metal complexes and fully solvated metal ions allowed the preparation of new magnetic materials namely, three bimetallic chains (**1**–**3**) and one three-dimensional compound (**4**) where the ruthenium unit adopts a bis-monodentate bridging mode through its two cyanide groups. Whereas **2** and **3** behave as magnetically isolated ferromagnetic chains without any magnetic ordering in the temperature range explored (1.9–295 K), **4** exhibits ferromagnetic ordering at very low temperatures (T_c = 5.5 K). The nature of the magnetic orbital of the low-spin ruthenium(III) complex *trans*-$[Ru(acac)_2(CN)_2]^-$ (which is roughly localized in the equatorial plane defined by the four acetylacetonate-oxygen atoms) accounts for the weak ferromagnetic coupling between Ru(III) and M(II) ions [M = Ni(II) (**1** and **3**) and Co(II) (**2** and **4**)] through the bridging cyano. Given that the spin density of this magnetic orbital on the cyanide groups is very poor, the use of this building block to get cyano-bridged species with strong magnetic interactions is ruled out. A more appropriate orientation

of the magnetic orbital of the cyano-bearing ruthenium(III) unit is required (changing the nature and/or number of the blocking ligands, for instance) to improve its efficiency as mediator of magnetic interactions.

Acknowledgements

This research was supported by The Ministerio Español de Educación y Ciencia (Projects CTQ2004-03633 and MAT2004-03112), the Generalitat Valenciana (Grupos 03/197), the Gobierno Autónomo de Canarias (Project PI2002/175) and the European Union (Project QueMolNa, MRTN-CT-2003-504880). Thanks are due to the University of Bergen and the NFR (Research Council of Norway) for grants allowing the purchase of X-ray equipment. Two of us (F.S.D. and L.M.T.) acknowledge the Gobierno Autónomo de Canarias and the Ministerio Español de Educación for predoctoral fellowships.

Appendix A. Supplementary data

Supplementary data associated with this article can be found, in the online version, at 10.1016/j.ccr.2005.11.018.

References

[1] K.R. Dunbar, R.A. Heintz, Prog. Inorg. Chem. 45 (1997) 283.
[2] M. Verdaguer, A. Bleuzen, V. Marvaud, J. Vaissermann, M. Seuleiman, C. Desplanches, A. Scuiller, C. Train, R. Garde, G. Gelly, C. Lomenech, I. Rosenman, P. Veillet, C. Cartier, F. Villain, Coord. Chem. Rev. 190–192 (1999) 1023.
[3] J. Cernak, M. Orendác, I. Potocnák, J. Chomic, A. Orendácova, J. Skorsepa, A. Feher, Coord. Chem. Rev. 224 (2002) 51.
[4] M. Pilkington, S. Decurtins, in: J.A. MacCleverty, T.J. Meyer (Eds.), Comprehensive Coordination Chemistry. II. From Biology to Nanotechnology, vol. 7, Elsevier, Amsterdam, 2004, p. 177.
[5] T. Mallah, S. Thiébault, M. Verdaguer, P. Veillet, Science 262 (1993) 1554.
[6] S. Ferlay, T. Mallah, R. Ouhaès, P. Veillet, M. Verdaguer, Nature (London) 378 (1995) 701.
[7] R. Garde, F. Villain, M. Verdaguer, J. Am. Chem. Soc. 124 (2002) 10531.
[8] W.R. Entley, G.S. Girolami, Science 268 (1995) 397.
[9] S.M. Holmes, G.S. Girolami, J. Am. Chem. Soc. 121 (1999) 5593.
[10] Ø. Hatlevik, W.E. Buschmann, J. Zhang, J.L. Manson, J.S. Miller, Adv. Mater. 11 (1999) 914.
[11] W. Dong, L.N. Zhu, H.B. Song, D.Z. Liao, Z.H. Jiang, S.P. Yan, P. Cheng, S. Gao, Inorg. Chem. 43 (2004) 2465.
[12] O. Sato, T. Iyoda, A. Fujishima, K. Hashimoto, Science 271 (1996) 49.
[13] O. Sato, S. Hayami, Y. Einaga, Z.Z. Gu, Bull. Chem. Soc. Jpn. 76 (2003) 443.
[14] O. Sato, T. Iyoda, A. Fujishima, K. Hashimoto, Science 272 (1996) 704.
[15] Z.Z. Gu, O. Sato, T. Iyoda, K. Hashimoto, A. Fujishima, Chem. Mater. 9 (1997) 1082.
[16] A. Bleuzen, C. Lomenech, V. Escax, F. Villain, F. Varret, C. Cartier dit Moulin, M. Verdaguer, J. Am. Chem. Soc. 122 (2000) 6648.
[17] C. Cartier dit Moulin, F. Villain, A. Bleuzen, M.A. Arrio, P. Sainctavit, C. Lomenech, V. Escax, F. Baudelet, E. Dartyge, J.J. Gallet, M. Verdaguer, J. Am. Chem. Soc. 122 (2000) 6653.
[18] D.A. Pejakovic, J. Manson, J.S. Miller, A. Epstein, J. Phys. Rev. Lett. 85 (2000) 1994.
[19] V. Escax, A. Bleuzen, C. Cartier dit Moulin, F. Villain, A. Goujon, F. Varret, M. Verdaguer, J. Am. Chem. Soc. 123 (2001) 12536.
[20] G. Champion, V. Escax, C. Cartier dit Moulin, A. Bleuzen, F. Villain, F. Baudelet, E. Dartyge, M. Verdaguer, J. Am. Chem. Soc. 123 (2001) 12544.
[21] R. Garde, F. Villain, M. Verdaguer, J. Am. Chem. Soc. 124 (2002) 10531.
[22] M. Mizuno, S. Ohkoshi, K. Hashimoto, Adv. Mater. 12 (2000) 1855.
[23] S. Ohkoshi, M. Mizuno, G. Hung, K. Hashimoto, J. Phys. Chem. B 104 (2000) 8365.
[24] M. Ohba, H. Okawa, Coord. Chem. Rev. 198 (2000) 313.
[25] H. Miyasaka, N. Matsumoto, H. Okawa, N. Re, E. Gallo, C. Floriani, Angew. Chem. Int. Ed. 34 (1995) 1446.
[26] K.V. Langenberg, S.R. Batten, K.J. Berry, D.C.R. Hockless, B. Moubaraki, K.S. Murray, Inorg. Chem. 36 (1997) 5006.
[27] H.Z. Kou, D.Z. Liao, P. Cheng, Z.H. Jiang, S.P. Yan, G.L. Wang, X.K. Yao, H.G. Wang, J. Chem. Soc., Dalton Trans. 1503 (1997).
[28] E. Colacio, J.M. Domínguez-Vera, M. Ghazi, R. Kivekäs, J.M. Moreno, A. Pajunen, J. Chem. Soc., Dalton Trans. (2000) 505.
[29] J.A. Smith, J.R. Galán-Mascarós, R. Clérac, K.R. Dunbar, Chem. Commun. (2000).
[30] G. Grasa, F. Tuna, R. Gheorghe, D.B. Leznoff, S.J. Rettig, M. Andruh, New J. Chem. 24 (2000) 615.
[31] G. Rogez, A. Marvilliers, E. Rivière, J.P. Audière, F. Lloret, F. Varret, A. Goujon, N. Mendenez, J.J. Girerd, T. Mallah, Angew. Chim. Int. Ed. 39 (2000) 2885.
[32] E. Colacio, M. Ghazi, H. Stoeckli-Evans, F. Lloret, J.M. Moreno, C. Pérez, Inorg. Chem. 40 (2001) 4876.
[33] V.V. Pavlishchuk, I.A. Koval, E. Goreshnik, A.W. Addison, G.A. van Albada, J. Reedijk, Eur. J. Inorg. Chem. (2001) 297.
[34] F. Bellouard, M. Clemente-León, E. Coronado, J.R. Galán-Mascarós, C.J. Gómez-García, F. Romero, K.R. Dunbar, Eur. J. Inorg. Chem. (2002) 1603.
[35] H.Z. Kou, B.C. Zhou, D.Z. Liao, R.J. Wang, Y. Li, Inorg. Chem. 41 (2002) 6887.
[36] C.P. Berlinguette, J.R. Galán-Mascarós, K.R. Dunbar, Inorg. Chem. 42 (2003) 3416.
[37] H. Miyasaka, H. Ieda, N. Matsumoto, K.I. Sugiura, M. Yamashita, Inorg. Chem. 42 (2003) 3509.
[38] E. Colacio, J.M. Domínguez-Vera, F. Lloret, A. Rodríguez, H. Stoeckli-Evans, Inorg. Chem. 42 (2003) 6962.
[39] S. Tanase, M. Andruh, N. Stanica, C. Mathonière, G. Rombaut, S. Golhen, L. Ouahab, Polyhedron 22 (2003) 1315.
[40] M.K. Saha, F. Lloret, I. Bernal, Inorg. Chem. 43 (2004) 1969.
[41] P. Alborés, L.D. Slep, T. Weyhermüller, L.M. Baraldo, Inorg. Chem. 43 (2004) 6762.
[42] J. Bendix, P. Steenberg, I. Søtofte, Inorg. Chem. 42 (2003) 4510.
[43] D.D. DeFord, A.W. Davidson, J. Am. Chem. Soc. 73 (1951) 1469.
[44] F.M. Crean, K. Schug, Inorg. Chem. 23 (1984) 853.
[45] W.F. Yeung, W.L. Man, W.T. Wong, T.C. Lau, S. Gao, Angew. Chem. Int. Ed. 40 (2001) 3031.
[46] T. Hasegawa, T.C. Lau, W.P. Schaefer, Inorg. Chem. 30 (1991) 2921.
[47] N.H. Pilkington, R. Robson, Aust. J. Chem. 23 (1970) 2225.
[48] A. Earnshaw, Introduction to Magnetochemistry, Academic Press, London, 1968.
[49] A.D. Becke, Phys. Rev. A 38 (1988) 3098.
[50] C. Lee, W. Yang, R.G. Parr, Phys. Rev. B 37 (1988) 785.
[51] A.D. Becke, J. Chem. Phys. 98 (1993) 5648.
[52] M.J. Frisch, G.W. Trucks, H.B. Schlegel, G.E. Scuseria, M.A. Robb, J.R. Cheeseman, J.A. Montgomery, T. Vreven Jr., K.N. Kudin, J.C. Burant, J.M. Millam, S.S. Iyengar, J. Tomasi, V. Barone, B. Mennucci, M. Cossi, G. Scalmani, N. Rega, G.A. Petersson, H. Nakatsuji, M. Hada, M. Ehara, K. Toyota, R. Fukuda, J. Hasegawa, M. Ishida, T. Nakajima, Y. Honda, O. Kitao, H. Nakai, M. Klene, X. Li, J.E. Knox, H.P. Hratchian, J.B. Cross, V. Bakken, C. Adamo, J. Jaramillo, R. Gomperts, R.E. Stratmann, O. Yazyev, A.J. Austin, R. Cammi, C. Pomelli, J.W. Ochterski, P.Y. Ayala, K. Morokuma, G.A. Voth, P. Salvador, J.J. Dannenberg, V.G. Zakrzewski, S. Dapprich,

A.D. Daniels, M.C. Strain, O. Farkas, D.K. Malick, A.D. Rabuck, K. Raghavachari, J.B. Foresman, J.V. Ortiz, Q. Cui, A.G. Baboul, S. Clifford, J. Cioslowski, B.B. Stefanov, G. Liu, A. Liashenko, P. Piskorz, I. Komaromi, R.L. Martin, D.J. Fox, T. Keith, M.A. Al-Laham, C.Y. Peng, A. Nanayakkara, M. Challacombe, P.M.W. Gill, B. Johnson, W. Chen, M.W. Wong, C. González, J.A. Pople, Gaussian 03, Revision C.02, Gaussian, Inc., Wallingford, CT, 2004.
[53] J.V. Ortiz, P.J. Hay, R.L. Martin, J. Am. Chem. Soc. 114 (1992) 2736.
[54] M. Dolg, H. Stoll, H. Preuss, R.M. Pitzer, J. Phys. Chem. 97 (1993) 5852.
[55] K.D. Dobbs, W.J. Hehre, J. Comput. Chem. 8 (1987) 880.
[56] P.J. Hay, W.R. Wadt, J. Am. Chem. Soc. 82 (1985) 270;
P.J. Hay, W.R. Wadt, J. Am. Chem. Soc. 82 (1985) 284.
[57] M. Dolg, U. Wedig, H. Stoll, H. Preuss, J. Phys. Chem. 86 (1987) 866.
[58] M.S. Gordon, J.S. Binkley, J.A. Pople, W.J. Pietro, W.J. Hehre, J. Am. Chem. Soc. 104 (1983) 2797;
K.D. Dobbs, W.J. Hehre, J. Comput. Chem. 8 (1987) 861.
[59] W.J. Hehre, R. Ditchfield, J.A. Pople, J. Am. Chem. Soc. 56 (1972) 2757;
V. Rassolov, J.A. Pople, M. Ratner, T.L. Windus, J. Chem. Phys. 109 (1998) 1223.
[60] A. Schaefer, A. Horn, R. Ahlrichs, J. Chem. Phys. 97 (1992) 2571.
[61] A. Schaefer, C. Huber, R. Ahlrichs, J. Chem. Phys. 100 (1994) 5829.
[62] J. Cano, P. Alemany, S. Alvarez, M. Verdaguer, E. Ruiz, Chem. Eur. J. 4 (1998) 476.
[63] E. Ruiz, J. Cano, S. Alvarez, P. Alemany, J. Am. Chem. Soc. 120 (1998) 11122.
[64] E. Ruiz, J. Cano, S. Alvarez, P. Alemany, J. Comput. Chem. 20 (1999) 1391.
[65] J. Cano, E. Ruiz, P. Alemany, F. Lloret, S. Alvarez, J. Chem. Soc., Dalton Trans. (1999) 1669.
[66] G.B. Bacskay, Chem. Phys. 61 (1981) 385.
[67] J.E. Carpenter, F. Weinhold, J. Mol. Struct. (TEOCHEM) 169 (1988) 41.
[68] A.E. Reed, L.A. Curtis, F. Weinhold, Chem. Rev. 88 (1988) 899.
[69] F. Weinhold, J.E. Carpenter, The Structure of Small Molecules and Ions, Plenum Press, 1988, p. 227.
[70] (a) SMART, Data Collection Software, Version 5.054, Bruker AXS Inc., Madison, WI, 1999;
(b) SAINT, Data Integration Software, Version 6.02a, Bruker AXS Inc., Madison, WI, 2001.
[71] (a) R.W.W. Hooft, COLLECT Nonius BV, Delft, The Netherlands, 1999;
(b) EVALCCD, J. Appl. Cryst. 36 (2003) 220.
[72] SADABS, Version 2.03, Bruker AXS Inc., Madison, WI, 2000.
[73] L.J. Farrugia, R.W.W. Hooft, J. Appl. Cryst. 32 (1999) 837.
[74] (a) G.M. Sheldrick, SHELXS-97, Acta Crystallogr., Sect. A 46 (1990) 467;
(b) G.M. Sheldrick, SHELXTL/PC, Version 6.12, Bruker AXS Inc., Madison, WI, 1998;
(c) G.M. Sheldrick, XP, Version 5.1, Bruker AXS Inc., Madison, WI, 1998;
(d) G.M. Sheldrick, SHELX-97, SHELXS-97, Program for Crystal Structure Refinement, Institut für Anorganische Chemie der Universität, Tammanstrasse 4, Göttingen, Germany, 1998.
[75] M. Nardelli, PARST95, J. Appl. Crystallogr. 28 (1995) 659.
[76] CrystalMaker 4.2.1, CrystalMaker Software, Bicester, Oxfordshire, UK.
[77] A. Cucos, G. Marinescu, Z. Zák, N. Stanica, M. Andruh, Rev. Roum. Chim. 47 (2002) 989.
[78] L. Toma, L.M. Toma, R. Lescouëzec, D. Armentano, G. De Munno, M. Andruh, J. Cano, F. Lloret, M. Julve, Dalton Trans. (2005) 1357.
[79] B.F. Hoskins, N.J. McLeod, H.A. Schaap, Aust. J. Chem. 29 (1976) 515.
[80] S.K. Mandal, L.K. Thompson, M.J. Newlands, E.J. Gabe, Inorg. Chem. 28 (1989) 3707.
[81] S.K. Mandal, L.K. Thompson, M.J. Newlands, E.J. Gabe, K. Nag, Inorg. Chem. 29 (1990) 1324.
[82] L.K. Thompson, S.K. Mandal, S.S. Tandon, J.N. Bridson, M.K. Park, Inorg. Chem. 35 (1996) 3117.
[83] G. Grasa, F. Tuna, R. Gheorghe, D.B. Leznoff, S.J. Rettig, M. Andruh, New J. Chem. 47 (2000) 989.
[84] B.F. Hoskins, G.A. Wiliams, Aust. J. Chem. 28 (1975) 2607.
[85] C.L. Spiro, S.L. Lambert, T.J. Smith, E.N. Duesler, R.R. Gagné, D.N. Hendrickson, Inorg. Chem. 20 (1981) 1229.
[86] S. Baggio, R. Baggio, A.W. Mombrú, Acta Crystallogr. C54 (1998) 1900.
[87] D. Britton, L.C. Thompson, R.C. Holz, Acta Crystallogr. C47 (1991) 1101.
[88] R. Chiozzone, R. González, C. Kremer, G. De Munno, D. Armentano, F. Lloret, M. Julve, J. Faus, Inorg. Chem. 42 (2003) 1064.
[89] T.F. Liu, D. Fu, S. Gao, Y.Z. Zhang, H.L. Sun, G. Su, Y.J. Liu, J. Am. Chem. Soc. 125 (2003) 13976.
[90] S.P. Watton, M.I. Davis, L.E. Pence, J. Rebeck Junior, S.J. Lippard, Inorg. Chim. Acta 235 (1995) 195.
[91] D.T. Corvin Jr, R. Fikar, S.A. Koch, Inorg. Chem. 26 (1987) 3079.
[92] M.J. Plater, M.R.J. St. Foreman, J.M.S. Skakle, R.A. Howie, Inorg. Chim. Acta 332 (2002) 135.
[93] E. Freire, S. Baggio, L. Suescun, R. Baggio, Acta Crystallogr. Sect. C: Cryst. Struct. Commun. 57 (2001) 905.
[94] E. Freire, S. Baggio, L. Suescun, R. Baggio, Aust. J. Chem. 53 (2000) 785.
[95] M. Uddin, M. Lakia-Kantouri, C.C. Hadjikostas, G. Voutsas, Z. Anorg. Allg. Chem. 624 (1998) 1699.
[96] A.J. Pallenberg, T.M. Marschner, D.M. Bamhart, Polyhedron 16 (1997) 2711.
[97] C. Tsalamis, A.G. Hatzidimitriou, M. Uddin, Inorg. Chim. Acta 249 (1996) 105.
[98] Y.H. Guo, Y.Q. Xue, R.G. Xiong, J.L. Zuo, X.Z. Yu, X.Y. Huang, Acta Crystallogr. Sect. C: Cryst. Struct. Commun. 52 (1996) 523.
[99] L. Ballester, A. Gutiérrez, M.F. Perpinan, T. Rico, E. Gutiérrez-Puebla, Polyhedron 13 (1994) 2277.
[100] N. Baidya, B.C. Noll, M.M. Olmstead, P.K. Mascharak, Inorg. Chem. 31 (1992) 2999.
[101] C.P. Bhasin, R. Bohra, G. Srivastava, R.C. Mehrotra, P.B. Hitchcock, Inorg. Chim. Acta 164 (1989) 11.
[102] R.J. Butcher, E. Sinn, Inorg. Chem. 16 (1977) 2334.
[103] R.J. Butcher, C.J. O'Connor, E. Sinn, Inorg. Chem. 18 (1979) 492.
[104] P.S. Shetty, Q. Fernando, J. Am. Chem. Soc. 92 (1970) 3964.
[105] H.S. Preston, C.H.L. Kennard, J. Chem. Soc. A (1969) 2682.
[106] F.E. Mabs, D.J. Machin, Magnetism and Transition Metal Complexes, Chapman & Hall, London, 1973, p. 115 (Chapter 5).
[107] S.L. Lambert, D.N. Hendrickson, Inorg. Chem. 18 (1979) 2683.
[108] E. Coronado, M. Drillon, R. Georges, in: C. O'Connor (Ed.), Research Frontiers in Magnetochemistry, Word Scientific Publishing, Singapore, 1993, p. 27.
[109] J.J. Borrás-Almenar, J.M. Clemente-Juan, E. Coronado, B.S. Tsukerblat, Inorg. Chem. 38 (1999) 6081.
[110] J.J. Borrás-Almenar, J.M. Clemente-Juan, E. Coronado, B.S. Tsukerblat, J. Comput. Chem. 22 (2001) 985.
[111] J.M. Herrera, A. Bleuzen, Y. Dromzée, M. Julve, F. Lloret, M. Verdaguer, Inorg. Chem. 42 (2003) 7052.
[112] P. Román, C. Guzmán-Miralles, A. Luque, J.I. Beitia, J. Cano, F. Lloret, M. Julve, S. Alvarez, Inorg. Chem. 35 (1996) 3741.
[113] L.M. Toma, F.S. Delgado, C. Ruiz-Pérez, R. Carrasco, J. Cano, F. Lloret, M. Julve, Dalton Trans. (2004) 2836.
[114] L. Toma, R. Lescouëzec, J. Vaissermann, F.S. Delgado, C. Ruiz-Pérez, R. Carrasco, J. Cano, F. Lloret, M. Julve, Chem. Eur. J. 10 (2004) 6130.